Genomic signatures of host-specific selection in a parasitic plant

Authors: Emily S. Bellis[1,2,3], Clara S. von Münchow[4], Calvins O. Odero[5], Alan Kronberger[1], Elizabeth Kelly[3], Tian Xia[3], Xiuzhen Huang[1,2], Susann Wicke[4, 5], Steven M. Runo[6], Claude W. dePamphilis[3], Jesse R. Lasky[3]

Target journal: AJB

Corresponding Author: Emily S. Bellis, ebellis@astate.edu

[1]Department of Computer Science, Arkansas State University, State University, AR, USA
[2]Center for No-Boundary Thinking, Arkansas State University, State University, AR, USA
[3]Department of Biology, Pennsylvania State University, University Park, PA, USA
[4]Institute for Biology, Humboldt University of Berlin, Berlin, Germany
[5] Späth-Arboretum of the Humboldt University of Berlin, Berlin, Germany
[6]Department of Biochemistry, Microbiology, and Biotechnology, Kenyatta University, Nairobi, Kenya

Manuscript received: _____; revision accepted: _____.

Running head: *Striga hermonthica* population genomics

ABSTRACT

***Premise*—**Parasitic plants and their hosts are emerging model systems for studying genetic variation in species interactions across environments. The parasitic plant *Striga hermonthica* (witchweed) attacks a range of cereal crop hosts in Africa. *Striga hermonthica* exhibits substantial genetic variation in host preference and in specificity versus generalism. Some of this variation is locally adapted, but the genetic basis of specialization on certain hosts is unknown.

***Methods*—**We present an alignment-free analysis of population diversity in *S. hermonthica* using whole genome sequencing (WGS) data for 68 individuals from western Kenya. We validate our reference-free approach with germination experiments and a *de novo* assembled draft genome.

Results—*K*-mer based analyses reveal high genome-wide diversity within a single field, similar to values between individuals collected 100 km apart or farther. Analysis of host-associated *k*-mers implicated genes involved in development of the parasite haustorium (a specialized structure used to establish vascular connections with host roots) and a potential role of chemocyanins in molecular host-parasitic plant interactions. Conversely, no phenotypic or genomic evidence was observed suggesting host-specific selection on parasite response to strigolactones, hormones exuded by host roots and required for parasite germination.

Conclusions—This study demonstrates the utility of WGS for plant species with large, complex genomes and no available reference. Contrasting with theory emphasizing the role of early recognition loci for genotype specificity, our findings support host-specific selection on later interaction stages, suggesting recurring host-specific selection each generation alternating with homogenizing gene flow.

Key words: population genomics, recurrent selective sweeps, agroecosystems, Orobanchaceae, host-parasite coevolution, chemocyanin

INTRODUCTION

Characterizing the genomic basis of adaptation to local biotic environments is a key challenge for evolutionary ecology (Ebert and Fields, 2020). Parasites and mutualists exert strong influences on host fitness, and may even constitute the predominant selective pressure shaping patterns of local adaptation in some systems (Fumagalli et al., 2011; Castellano et al., 2019). Compared to abiotic environmental gradients, adaptation to biotic environments may be characterized more frequently by selection on fewer mutations of large effect, due to selection on a more rapidly changing adaptive landscape (Wilfert and Schmid-Hempel, 2008; Louthan and Kay, 2011). However, many host-parasite and host-mutualist systems involve a complex

multi-step infection process including many stages of interaction between host and symbiont derived molecules (Hall et al., 2017).

An outstanding question is whether adaptation to local biotic environments occurs most often via selection on genes involved during initial infection stages, or whether genetic variation at later stages of the interaction is also frequently maintained. The expectation from theoretical studies is that initial recognition loci are more likely than downstream effector loci to contribute to host genotype by parasite genotype interactions (G_H x G_P) and correspondingly, local adaptation (Nuismer and Dybdahl, 2016). The first prediction, that recognition loci contribute more to G_H x G_P, is supported by empirical studies of the waterflea *Daphnia magna* and its bacterial parasite *Pasteuria ramosa* (Hall et al., 2017). In this system, most of the genetic variance in parasite infection was associated with a single major effect QTL linked to the early stage of parasite attachment (Hall et al., 2019). In contrast, many different QTLs of smaller effect were associated with later stages, highlighting the potential for independent evolution of traits involved in different stages of the infection process (Hall et al., 2019). Supporting the second prediction that selection on recognition traits often underlies local adaptation (Nuismer and Dybdahl, 2016), studies of plant pathosystems have revealed reciprocal coevolutionary selection on host resistance (R) genes and parasite avirulence genes, for example in the flax-flax rust system (Ravensdale et al., 2011; Thrall et al., 2012). However, a high degree of genotype specificity has also been observed for many host-parasite systems characterized by more quantitative mechanisms of resistance (Poland et al., 2009). For host-parasite interactions characterized by quantitative genetic architectures, we still know little regarding the genetic basis of local adaptation in natural populations and the extent to which initial vs. later infection stages contribute to G_H x G_P.

An emerging model system for studying spatial pattern and process in coevolutionary genomics is the parasitic plant *Striga hermonthica* and its cereal hosts. In contrast to *Striga gesneriodes,* which parasitizes cowpea via a qualitative gene-for-gene mechanism, host

resistance to *S. hermonthica* is highly polygenic (Li and Timko, 2009; Timko et al., 2012) with at least one large effect locus (Gobena et al., 2017). *Striga hermonthica* parasitizes grass hosts including sorghum, maize, rice, and millets and is one of the greatest biotic constraints to food security in Africa (Ejeta, 2007; Spallek et al., 2013; Savary et al., 2019). An individual *S. hermonthica* plant can produce thousands of seeds that may survive in the soil for a decade or more under optimal conditions (Bebawi *et al.* 1984; but see Gbèhounou *et al.* 2003).

Parasite seeds germinate by detecting strigolactones (SLs), hormones exuded from host roots under nutrient-deficient conditions that also stimulate host interactions with beneficial mycorrhizal fungi (Akiyama et al., 2005). Parasite perception of SLs is mediated through binding to paralogs of KARRIKIN INSENSITIVE 2 (KAI2), known as HYPOSENSITIVE TO LIGHT (HTL) proteins. SL receptors of the *KAI2d* clade rapidly expanded and diversified during the transition to parasitism in the Orobanchaceae, a plant family that includes thousands of mostly parasitic species (Conn et al., 2015). For example, the ~600 Mb genome of *Striga asiatica* contains 21 *KAI2* genes, many of which occur as tandem duplications (Yoshida et al., 2019). *Striga hermonthica* may contain 13 or more *KAI2* paralogs (Nelson, 2021), including 11 for which the binding affinity for diverse SLs has been extensively characterized (Toh et al., 2015; Tsuchiya et al., 2015). The continent-wide distribution of host-specific *S. hermonthica* populations suggests adaptation to their local host communities, via generalization where diverse hosts are available and specialization where a particular host is common (Bellis et al., 2021). Given the low germination of millet- and sorghum-specific *S. hermonthica* populations in response to root exudates from the alternate host (Parker and Reid, 1979), it is possible that at least some of this host-specificity results from natural selection on SL perception. Host-specific germination of *Striga* species could result from expanded SL response by different *KAI2* paralogs, or evolutionary fine-tuning of SL perception if some SL receptors instead function to inhibit germination (Nelson, 2021).

Following SL perception and parasite germination, host-derived phenolic compounds induce formation of the haustorium, the specialized multicellular feeding structure used by parasitic plants to invade host tissues (Cui et al., 2018). Intrusive cells of the haustoria invade host tissues to form direct connections with host vasculature (Masumoto et al., 2021). Water, nutrients, and other molecules including mRNA (Kim et al., 2014), small RNA (Shahid et al., 2018), DNA (Yang et al., 2019), and proteins (Liu et al., 2020; Shen et al., 2020) are directly transferred through haustorial connection. In addition to natural variation in low germination stimulation (Dayou et al., 2021; Mallu et al., 2021), post-germination host resistance in *Striga hermonthica* is often apparent across diverse hosts, for example due to induction of an intense hypersensitive response, formation of a mechanical barrier, or failure of the parasite to form vascular connections (Mbuvi et al., 2017; Mutinda et al., 2018; Kavuluko et al., 2020). Much of this genetic variation in natural resistance may result from host populations' local adaptation to parasitism across the range of *Striga hermonthica* (Bellis et al., 2020).

Extensive genetic and germplasm resources have enabled broad-scale studies of local adaptation in *Striga* hosts (Bellis et al., 2020), but understanding reciprocal adaptation in parasite populations is challenged by paucity of genomic data for *S. hermonthica.* At the population-scale, restriction-site associated DNA sequencing (RAD-Seq) and analysis of polymorphism in transcriptomes have begun to shed light on population level diversity in these parasites (Unachukwu *et al.* 2017; Lopez *et al.* 2019). However, reduced representation approaches pose difficulties if only a fraction of host genome diversity is tagged by RAD-Seq markers (Lowry et al., 2017) or (in the case of transcriptomes) if genes under selection are not expressed in sequenced tissues. Like other parasitic angiosperms, *S. hermonthica* is characterized by a larger genome than non-parasitic relatives (Lyko and Wicke, 2021), with estimated size of ~1 Gb (1C = 0.9 Gb; Yoshida *et al.* 2010) or greater (1C = 1.4 Gb; Estep *et al.* 2012). *Striga hermonthica* is a highly heterozygous obligate outcrosser, posing additional challenges for genome assembly and reference-based approaches. Here, we provide a

reference-free analysis of population-scale diversity in *S. hermonthica,* based on whole genome sequencing (WGS) data. Using a unique alignment-free bioinformatic approach, we identify genetic variation associated with host-specific parasitism in natural populations and investigate signatures of selection surrounding these loci. Based on these findings, we evaluate the hypothesis that adaptation to local host populations results from selection on genes involved in early stages of the interaction (SL perception) against the alternative that selection on genes involved in later stages is primarily responsible.

MATERIALS AND METHODS

Sample Collection—Seeds and leaf tissue were collected from *S. hermonthica* individuals in July 2018 from six locations in western Kenya (Table S1). Two plots with *S. hermonthica* parasitizing different host species were sampled at each location, chosen as close as possible and in most cases, from nearby plots on the same farm (i.e. within 15 meters). Per plot, twelve *S. hermonthica* individuals were chosen haphazardly, with effort taken to sample individuals distributed evenly throughout the plot. This sampling design was expected to result in the selection of individuals from the same interbreeding population that are relatively homogeneous across their genetic background due to high rates of gene flow among neighboring plots. However, sampling mature plants could allow for identification of loci under selection for parasitism on a specific host due to a single generation of selection. Individuals were photographed before collection and images for representative individuals at each site uploaded to iNaturalist. Three to four leaves per individual were sampled directly into silica gel, before collection of the whole individual into separate paper bags. Plants were dried in paper bags before harvesting and manual cleaning of seeds. Cleaned seeds were shipped to Penn State for germination rate experiments and stored in individual 2 mL microcentrifuge tubes at room temperature prior to experiments. Five voucher specimens (ESB collection numbers 2018.1 to 2018.5) were deposited in the collection of the East African Herbarium (EA).

Whole genome sequencing—For samples collected in 2018, whole genome sequencing was performed for a subset of 68 *S. hermonthica* individuals. This included all 24 individuals collected from adjacent plots of finger millet and maize in Kisii, all 24 individuals collected from adjacent plots of sorghum and maize in Homa Bay, and five individuals (two or three per plot) from four additional locations. DNA was extracted from silica-dried leaf tissue in the USDA APHIS quarantine facility at the Pennsylvania State University using the E.Z.N.A. Plant DNA DS Mini Kit (Omega Bio-tek, Norcross, Georgia, USA) according to the manufacturer's protocol. Genomic library preparation and paired-end 150 bp sequencing was carried out by the Texas A&M AgriLife Genomics and Bioinformatics Service, on a single lane of a NovaSeq 6000 S4 flow cell.

Population structure—We followed a reference-free approach to evaluate population genomic patterns among sequenced samples. Raw reads that could be classified as plant-derived were identified using Kraken 2 (Wood et al., 2019), based on a custom database built from the complete set of plant genomes and proteins in the NCBI RefSeq collection, sequences from 472 Mbp of the *Striga asiatica* genome (Yoshida et al., 2019) and *S. hermonthica* transcriptome sequences (build StHeBC4) from the Parasitic Plant Genome Project II (Yang et al., 2014). Classified sequences were trimmed using BBduk from BBTools (Bushnell, n.d.), removing sequence on the ends of reads with low quality (qtrim=rl trimq=20 minlen=50) or 3' matches to adapters (k=23 mink=11 hdist=1 tpe tbo ktrim=r). To reduce bias associated with differences in per-sample read depth, reads were downsampled to 5.2 Gbp with BBTools Reformat.

Mash, a dimensionality reduction technique based on the MinHash algorithm, was used to estimate genetic distance between samples based on resulting read sets (Ondov et al., 2016). *Mash* previously showed improved performance compared to alignment-based methods

for estimating pairwise genetic distance for polyploid plant genomes using simulated and real data (VanWallendael and Alvarez, 2020). We used a *k*-mer size of 31, removing *k*-mers with less than 2 copies but increasing the sketch size to 1×10^7 to account for a larger volume of input data. Principal Coordinates Analysis was performed in R version 4.0 with the pcoa function of the 'ape' package (Paradis and Schliep, 2019). A smaller *k*-mer size (*k*=21) was also tested but did not alter clustering patterns in PCoA. Correlation between the genetic distance matrix and the geographic distance matrices, calculated with 'geodist', was determined using a Mantel test (Padgham and Sumner, 2021).

Germination experiments—Seed germination was assayed in the USDA-APHIS-permitted quarantine lab at Pennsylvania State University (permit no. P526P-21-04540). A detailed step-by-step protocol is available from protocols.io repository (Bellis and Kelly, 2019), following the modifications for testing seeds collected from individual plants. Briefly, seeds were surface sterilized for 10 minutes in 1.5 mL microcentrifuge tubes with a 0.5% sodium hypochlorite solution before preconditioning for 12 days at 30°C in separate wells of foil-wrapped 12-well culture plates, with three technical replicates per unique germination stimulant and parasite genotype combination. Germination counts were performed 3 days after addition of germination stimulants. Tested germination stimulants included (+)5-deoxystrigol (Olchemim, Olomouc, Czech Republic; CAS: 151716-18-6) or (±)orobanchol (Olchemim; CAS: 220493-64-1) at 0.01 µM and (±)-GR24 (Chempep, Wellington, Florida, USA; CAS: 76974-79-3) at 0.2 µM. GR24 is a synthetic strigolactone analog commonly used in laboratory germination studies of parasitic plants as a positive control. 5-deoxystrigol is one of the major SLs produced by compatible grass hosts (Awad et al., 2006) and is a potent stimulator of parasite germination whereas orobanchol is a more dominant SL among dicot hosts (Yoneyama et al., 2008) and is a less potent stimulator of *S. hermonthica* germination for certain genotypes (Cardoso et al., 2014). Specifically, *S. hermonthica* tested populations from Mali and Niger germinate poorly in

response to orobanchol (Haussmann et al., 2004; Bellis et al., 2020) whereas Kenyan *S. hermonthica* show a greater ability to germinate in response to exudate from sorghum hosts carrying loss-of-function mutations at the sorghum resistance locus *LOW GERMINATION STIMULANT 1 (LGS1),* which results in high amounts of orobanchol rather than 5-deoxystrigol in root exudates (Gobena et al., 2017).

In addition to seed collections kept separately from individual plants, we also included tests of bulk seed collected from the Kibos population that were confirmed to have high germinability in our previous experiments (Bellis et al., 2020). We used a generalized linear mixed model (GLMM) with a random effect of *S. hermonthica* genotype (of the parent plant) to compare differences in germination rate among sites, hosts, and treatments (orobanchol vs. 5-deoxystrigol). GLMMs were implemented in R version 4.0 with the lme4 package (Bates *et al.* 2015).

Host-specific differentiation—We next sought to identify particular genomic regions differentiated between parasites growing on different hosts. This analysis targeted parasite populations from Homa Bay or Kisii, for which we sequenced DNA from parasites for two different hosts on the same farm from immediately adjacent plots. For the Kisii population, the dataset included individuals from finger millet and maize, whereas for the Homa Bay population the dataset included parasites from sorghum and maize (n = 12 from each host species; 48 individuals total). Counts for k-mers of length 31 were summarized across sequenced individuals using HAWK (Rahman et al., 2018) and used to calculate the fixation index, G_{ST} (Nei and Chesser, 1983), for each k-mer using custom Python scripts. G_{ST} is a generalization of the widely used fixation index F_{ST} applicable to non-diploid loci (Nei, 1973). To extend G_{ST} to our reference-free genotyping approach, at each k-mer we considered two allelic states (present or absent) where the k-mer was marked as present in an individual if it was counted at least once or absent if it was not observed at all.

239 To gather functional information for host-associated *k*-mers, 31-mers with G_{ST} above 0.5
240 were extracted and assembled into longer contigs using ABYSS 2.0.2, specifying a *k*-mer length
241 of 29 for assembly (Jackman et al., 2017). Assembled contigs were then queried against contigs
242 from two published *S. hermonthica* transcriptome assemblies using BLAST optimized for short
243 sequences (blastn-short). Transcriptome assemblies in our BLAST database included StHeBC4
244 (265,694 scaffolds covering 369.7 Mb) from the Parasitic Plant Genome Project (Westwood et
245 al., 2012) and Sh14v2 (81,559 scaffolds covering 83.9 Mb) from Yoshida *et al.* (2019).
246 Annotations are based on the top hit from the Sh14v2 transcriptome.
247 Contigs assembled from host-associated *k*-mers were further studied by mapping
248 cleaned sample reads to mRNA reference sequences, following the strategy from (Therkildsen
249 and Palumbi, 2017). Mapping to a transcriptome reference has the potential to introduce errors
250 in SNP calling due to intron/exon boundaries and the short length of transcripts, so we restricted
251 this analysis to a small set of loci for which alignments could be manually inspected. Sequences
252 in our reference included three transcripts with potential functions in haustorium development
253 (StHeBC4_h_c11261_g0_i1, StHeBC4_p_c12587_g2_i1, StHeBC4_u_c12903_g27039_i4; see
254 Results). The reference also included transcript sequences for a set of 11 previously
255 characterized *S. hermonthica* strigolactone receptors [GenBank accession numbers KR013121
256 - KR13131] (Tsuchiya et al., 2015). High quality, contaminant-filtered reads were mapped to the
257 reference transcriptome using BWA-MEM (Li, 2013), and alignments with low quality were
258 removed using samtools view (-q 20) (Li et al., 2009). Allele frequencies for each site in the
259 reference transcriptome were estimated based on genotype likelihoods using ANGSD, ignoring
260 low quality bases (-minQ 25) and allowing reads for which only one end mapped (-
261 only_proper_pairs 0) (Kim et al., 2011; Korneliussen et al., 2014). Sites with information for
262 fewer than nine of twelve individuals in the population were excluded, and the difference in
263 estimated allele frequency between parasite populations on different hosts was visualized with
264 R version 4.0 (R Core Team, 2020). This strategy was used to filter false SNP calls due to

errors in mapping DNA-derived reads to a transcriptome reference, since these SNPs should be observed as a fixed difference from the reference that occurs in both populations. We further investigated genes with potential structural variation by extracting reads aligned to the transcript reference and their unmapped pairs and reassembling them with ABYSS (k=51) (Jackman et al., 2017).

Validation of* k*-mer-based approaches—To investigate patterns of selection surrounding putative host-associated loci and validate findings from reference-free analyses, we also mapped reads generated for *S. hermonthica* to a draft reference assembled specimen, grown *ex situ* from seeds collected on maize in the Irimbi district of Southern Uganda (specimens voucher deposited at MSUN). DNA was extracting from developing leaves and inflorescences of one individual using a modified 1x CTAB-protocol with subsequent PEG-8000 precipitation and purification (Wicke et al., 2016). Genomic libraries were sequenced on an Illumina HiSeq 2000 in 101 bp paired-end mode at Eurofins GATC Biotech GmbH (Constance, Germany). Additional data were generated to a targeted depth of 110X using the HiSeq 2500 platform using the HiSeq SBS Kit v4 at Eurofins GATC Biotech GmbH, for which DNA from the original extract was subjected to Φ29-polymerase based whole-genome amplification. Whole genome-amplified DNA was size-selected for >20 kb fragments on 1% low-melting point agarose and purified using an agarose digest-based purification from gel with subsequent ethanol/sodium acetate precipitation (Wicke et al., 2013). For the final assembly, we employed Trimmomatic v0.36 (Bolger et al., 2014) to remove adapters and retain only sequences longer than 36 bp with an average per-base quality above 15 (“ILLUMINACLIP:TruSeq3-PE.fa": 2:30:10 SLIDINGWINDOW:4:15 MINLEN:36). The quality-trimmed data were assembled using SPAdes v3.10.1 with *k*-mer sizes of 21, 33, 55, and 77 (Bankevich et al., 2012). Assembly quality was ascertained using Quast v4.5 (Gurevich et al., 2013) with default parameters for eukaryotes. The resulting assembled contigs were contaminant-filtered, for which we ran a

nucleotide BLAST search of all contigs against the non-redundant nucleotide database (access date: 10.07.2017) using BLAST+ v2.6 with an e-value of $1E10^{-4}$. Only contigs with the three best hits matching to green land plants (Viridiplantae) were retained.

After removing scaffolds shorter than 500 bp from the reference, high quality sequences from each *S. hermonthica* individual were mapped using BWA-MEM v0.7.17 (Li, 2013). Sequences mapping with quality less than 20 were excluded using SAMtools v1.10 (Li et al., 2009). Tajima's D was calculated in non-overlapping windows of 1-kb using ANGSD v0.935 based on the folded site frequency spectrum and including reads where only one end mapped (-only_proper_pairs 0), to account for the highly fragmented nature of the assembly (Korneliussen et al., 2014). F_{ST} was also calculated in non-overlapping windows with ANGSD, using the SAMtools method for calculating genotype likelihoods. Genome-wide mean values of Tajima's D were determined by fitting an intercept-only linear mixed model to window estimates of F_{ST} or Tajima's D, including a random effect of 'contig' to account for increased correlation among measurements from nearby genomic regions, with the R package lme4 (Bates et al., 2015). An empirical *P*-value for Tajima's D for the contig containing the chemocyanin was calculated based on the number of 10,000 randomly sampled windows of size matching the assembled length of the contig (1-kb) with values more extreme than the observed value.

To validate the presence/absence polymorphism for the chemocyanin gene, we performed PCR using primers designed from the reassembled 'finger millet' allele (Primer Set A: 5'-AAGATTGCGGTTACCACCAG-3' and 5'-TCTCGATCCTTTTGGAATGG-3') and the transcript reference (Primer Set B: 5'- CAGGAGCAAGTAGAGTAGAGCA-3' and 5'-TGGGGAAAGAGGTAGTGCAA-3'). PCR was performed with DreamTaq DNA Polymerase 2x Mastermix (ThermoFisher, Waltham, Massachusetts, USA) under the following cycling conditions: 95°C for 3 min; 30 cycles of 95°C (30 s), 50.3°C (30 s), 72°C (60 s); 72°C for 5 min.

RESULTS

317 ***Sequencing—***For the 68 Kenyan samples, on average 80% of reads per library were
318 classified as plant-derived using Kraken 2 (range: 71-86%). The majority of classified reads
319 matched the *S. hermonthica* transcriptome (mean: 46%) or the *S. asiatica* genome (mean:
320 30%). After quality and adapter trimming, on average 7.7 Gigabase pairs of plant-derived
321 sequence data remained per sample (range: 5.2-11.7 Gbp). Given flow cytometry estimates of
322 the genome size of *S. hermonthica* ranging from 1C = 0.9 Gb (Yoshida et al., 2010) to 1C = 1.4
323 Gb (Estep et al., 2012), this sequencing effort corresponds to an approximate average depth of
324 5.5x to 8.6x read coverage per base for each sample.
325
326 ***Population structure***—In contrast to previous studies based on microsatellite markers
327 (Gethi et al., 2005) but consistent with results from GBS (Unachukwu et al., 2017), our analyses
328 suggest that geography is a primary factor shaping population structure in *S. hermonthica* from
329 western Kenya. Principal Coordinates Analysis (PCoA) based on *k*-mers indicated high genetic
330 diversity within populations, with only subtle differentiation of populations from the same farm
331 collected from different hosts (Fig. 1). Greater correlation was observed between genetic and
332 geographic distance than expected by chance (p = 0.001, Mantel test), and patterns of genetic
333 variation were consistent with those expected under isolation by distance (Fig. 1F). Although
334 populations were structured by distance, within-population diversity was very high at the
335 geographic scale investigated. Many individuals exhibited a comparable range of pairwise
336 genetic diversity within a single field (*k*-mer distance ranging from 0.0216 - 0.0286; n = 572
337 pairwise comparisons) as between individuals sampled more than 100 km apart (*k*-mer distance
338 ranging from 0.0242 - 0.0286; n = 336 pairwise comparisons; Fig. 1F).
339
340 ***Germination rate variation***—Previous studies have suggested that in contrast to other
341 locations in Africa, *S. hermonthica* populations from western Kenya demonstrate a generalist
342 germination response to strigolactones (Haussmann et al., 2004; Bellis et al., 2020). However,

Striga germination tests are typically conducted with bulk seeds collected from many individuals in a field, potentially masking individual-level variation that could be segregating with respect to parasitism on different hosts, for example if a generalist population is composed of individuals that specialize on different resources (Bolnick et al., 2002).

To characterize individual-level variation in western Kenyan *S. hermonthica,* we conducted controlled germination tests in the USDA-permitted quarantine facility at Pennsylvania State University. Positive controls with bulk seed (collected in the Kibos region) and 0.2 µM of the artificial strigolactone GR24 indicated good germinability for positive controls (66.5%), and no germinated seeds were observed in wells with only sterile water. Compared to the higher concentration of GR24, bulk seed showed slightly lower germination rates in response to 0.01 µM of the natural SLs orobanchol (51.0%) and 5-deoxystrigol (55.7%) indicating that the concentrations of orobanchol and 5-deoxystrigol used in the individual-level experiment should produce strong but sub-maximal germination responses.

We did not find significant host-associated germination variation among seeds collected from individual parasites on different hosts (Table S1; Fig. 2). After accounting for treatment and site, host-of-origin was not a statistically significant effect in our model ($P = 0.247$; likelihood ratio test for test of full vs. reduced GLMM). Comparing individuals from Kisii to Homa Bay, the probability of germination was 30% lower ($P = 0.04$; GLMM with fixed effects of 'Site' and 'Treatment') and 15% lower in response to orobanchol than to 5-deoxystrigol ($P = 0.004$; GLMM).

Host-associated loci—Germination tests did not support host-specific differences in strigolactone response in these populations. However, it is possible that host-specific selection could still leave detectable signatures at the genetic level. We identified host-associated genetic variation without a reference using a *k*-mer based approach. Highly differentiated *k*-mers were defined as those having $G_{ST} > 0.5$ (Fig. S2). A greater proportion of *31*-mers were highly

differentiated for parasites on finger millet vs. maize hosts in Kisii (4.8% of *31*-mers) compared to sorghum vs. maize hosts in Homa Bay (0.6% of *31*-mers; Fig. S1).

Highly differentiated *31*-mers were then assembled into longer contigs for follow-up analysis. For the Homa Bay population (maize vs. sorghum hosts), 42 contigs were assembled ranging in length from 58 to 91 bp. Sixteen of these contigs had good BLAST hits to the transcriptome database, with >85% identity over at least 45 bp (Table 1). For the Kisii population (finger millet vs. maize hosts), highly differentiated *k*-mers assembled into 469 contigs with length ranging from 29 to 211 bp. Of these, 241 had good BLAST hits to transcripts in our database (Table S2).

Of particular interest to our investigation were host-specific contigs with high levels of similarity to known *Striga* parasitism genes including SL receptors and genes involved in haustorium development. We first searched for similarity to a set of 11 *S. hermonthica* strigolactone receptors that vary in their binding affinity for diverse strigolactones [GenBank accession numbers KR013121 - KR13131] (Tsuchiya et al., 2015). We observed only one likely spurious match to *ShHTL2* (87% similarity over 23 bp) and no hits to any of the 21 *KAI2* paralogs from the *Striga asiatica genome* (Yoshida 2019). In follow-up analyses based on alignments to reference *ShHTL* transcripts, only one site in *ShHTL6* had an estimated difference in allele frequency between parasites on finger millet and maize exceeding 0.5 (Fig. S2). This polymorphism occurred at position 457 and does not result in an amino acid change. Together, we find little phenotypic or genomic evidence supporting host-specific differentiation for loci involved in perception of strigolactones in these populations.

In contrast, several assembled host-specific contigs had good matches to loci implicated in development of haustoria (Fig. 3). Annotated transcripts included a 60 bp contig with >98% similarity over its full length to a transcript annotated as *SUPPRESSOR OF G2 ALLELE SKP1* (*SGT1*) (Table S1). *SGT1* was among the top upregulated genes in haustoria of the root parasitic plant *Thesium chinense* and was hypothesized to be important for generating auxin

response maxima during haustorium development (Ichihashi et al., 2017). In *S. hermonthica,* it is also highly expressed in imbibed seeds (Stage 0) and in haustoria attached to host roots (Stage 3; Fig. 3D). Parasitism on different hosts was associated with genetic structural variation in *SGT1*, with two <100 bp regions often absent from parasites on sorghum but present for parasites on maize and finger millet. We also identified a 59 bp contig with 96% similarity over its full length to a transcript annotated as a pectin methylesterase; pectin methylesterases have previously well-characterized functions in developing haustoria (Yang et al., 2014). The pectin methylesterase transcript was not expressed in parasites grown on sorghum in most stages, but exhibited low, non-zero expression in *S. hermonthica* seedlings after exposure to a haustorium inducing factor (mean TPM = 0.03). We did not identify evidence for structural variation in this gene in transcript-aligned reads, though strong differentiation between individuals from finger millet (AF = 0.65) and maize (AF = 0.03) verified the signal observed from the *k*-mer association analysis.

Two additional assembled host-differentiated contigs of 113 bp and 103 bp had 99% and 97% similarity, respectively, over their full length to separate regions of a single transcript annotated as a precursor of chemocyanin (Table S2). Chemocyanins may be of particular interest due to the evolutionary co-option of many pollen tube genes by parasitic plants for haustorium development (Yang et al., 2014) and the key role of chemocyanin as an attractant for directing pollen tube growth (Kim et al., 2003). The chemocyanin transcript was present in a previously identified list of *S. hermonthica* “core parasitism” genes with highest expression in stages 3 and/or 4 of haustorial development (Yang *et al.* 2014; Fig 3B). It was also highly expressed in cells at the host-parasite interface in a study that used laser capture microdissection to characterize gene expression in the *S. hermonthica*-sorghum interaction (Honaas et al., 2013).

Alignment of our DNA sequences to the chemocyanin transcript reference revealed host-associated structural variation (Fig. 3A). PCR-based confirmation indicated 500 bp or more of

genome sequence directly upstream of the 5' end of the transcript was completely missing from parasites on maize, suggesting potential impact on variation in gene expression levels. The fragmented nature of the draft genome assembly precluded our ability to design PCR primers completely spanning the deletion, but PCR banding patterns showed a characteristic absence of the region in individuals having the allele more common on finger millet (Fig. S4), and a diversity of deletion alleles at this site (Fig. S5). Using just sequences for individuals parasitizing finger millet, we reconstructed a 934 bp contig, from reads that mapped to the transcript reference and their unmapped pairs. Alignments to this 'finger millet' allele confirmed its presence in 9/12 individuals from Kisii parasitizing finger millet (AF = 0.75) and 0/12 parasites on maize (Table S3). Among all individuals sequenced in our study, the allele is present at lowest frequency in maize parasites (AF = 0.14; *n* = 35) and intermediate frequency for parasites on sorghum (AF = 0.22; *n* = 18); and sugarcane (AF = 0.33; *n* = 3).

***Validation of* k*-mer-based approaches*—**To further investigate signatures of selection in the context of genome-wide patterns, we assembled a draft genome for *S. hermonthica* from South Uganda. The total length of the assembled genome after filtering was 1,431 Mbp over 12,155,247 contigs, with a maximum contig length of 37.5 kb. The assembly was highly fragmented with the largest 1.69 million contigs accounting for 50% of the assembly, and the length of these contigs ≥ 110 bp (N/L50 = 1690935/110). Nevertheless, sequences of interest were present on contigs long enough to allow for further interrogation. Specifically, the assembled chemocyanin transcript for the finger millet allele had 97.8% identity over 918 bp to a single contig of 1,055 bp (NODE_132909_length_1055_cov_32.632), and no other close hits. After removing contigs shorter than 1 kb, 307026 scaffolds with a total length of 479 Mbp remained. A Tajima's D value of -1.7 in the Kisii population indicated a significant excess of low-frequency polymorphism (empirical *P*-value = 0.009) for the chemocyanin contig in the *de novo*

446 assembly compared to the genome-wide value of 0.11 ± 0.013 (mean ± std. error for non-
447 overlapping 1-kb windows; linear mixed effects model).
448
449 **DISCUSSION**
450 Agricultural weeds are increasingly recognized as important model systems for
451 addressing key questions in evolution and ecology (Vigueira et al., 2013; Baucom, 2019). In
452 particular, compared to many other systems, parasitic weeds offer particular advantages for the
453 study of coevolution including well-developed genomic and germplasm resources for their hosts,
454 high quality distributional data, and a rich literature describing variation in species interactions
455 over many decades (Bellis et al., 2020, 2021). Yet, despite recent advances in genome
456 sequencing for parasitic plants, evolutionary analyses particularly for species with large,
457 complex genomes (e.g. >1 Gb) remain a challenge (Lyko and Wicke, 2021). Consequently,
458 previous population-level diversity studies for *S. hermonthica*, one of the most damaging
459 parasitic plants in agriculture, have used reduced representation approaches (Unachukwu et al.,
460 2017; Lopez et al., 2019). However, reduced representation approaches such as RAD-seq may
461 miss signatures of selection that are highly localized in the genome (Lowry et al., 2017; Lou et
462 al., 2021), and transcriptomes fail to provide information regarding non-coding regions of the
463 genome, which also generate phenotypic diversity. As the cost of sequencing continues to
464 decrease, whole genome resequencing coupled with alignment-free bioinformatic approaches
465 can provide a promising alternate approach for surveying population genomic diversity (Voichek
466 and Weigel, 2020). Here, we report some of the first publicly available WGS data for field-
467 sampled individuals of the parasitic weed *Striga hermonthica*. Our analyses underscore high
468 within-population genomic variation and implicate host-specific selection on genes involved
469 during parasite attachment and haustorial development.
470 Perhaps surprisingly, we find little genomic or phenotypic evidence for host-specific
471 selection on strigolactone perception variation in the studied populations. Specifically, one may

expect selection on perception loci to be relatively strong, particularly since *S. hermonthica* is an obligate parasite and so the costs of germination in the absence of a suitable host are high. The genomes of *Striga* spp. include a diverse repertoire of strigolactone receptors, each with variable affinity for different SLs (Tsuchiya et al., 2015; Yoshida et al., 2019), providing many potential targets for selection on SL response variation. One possibility is that these receptors are now subject to purifying selection in western Kenya, rather than diversifying selection expected if SL perception variation is strongly linked to fitness variation across different hosts. Environmental niche models from our previous study (Bellis et al., 2021) predict highest habitat suitability for maize parasitism across sampling locations in our study (mean habitat suitability: 0.92) but lower suitability for sorghum and pearl millet (0.46 and 0.03, respectively). Strong selective pressure for maize parasitism may contribute to the generalist germination response observed in western Kenya. Another possibility is that the particular host genotypes studied here may overlap in SL exudation profile enough that selection on parasite germination rate variation is not strong in these natural field populations. For example, while zealactones appear to be uniquely produced by maize (Charnikhova et al., 2017), some varieties also naturally produce sorgomol and 5-deoxystrigol in high quantities (Yoneyama et al., 2015), strigolactones common in sorghum root exudate that promote strong germination response in *S. hermonthica*.

A third explanation is that SL perception is important for reciprocal selection and coevolution only in some populations across the range of *S. hermonthica.* This explanation is consistent with the idea of coevolutionary hotspots, where there is reciprocal selection among coevolving species (Thompson, 2005), but with the genetic targets of selection involving different stages of the infection process in different locations. In western Kenya, for example, coevolutionary hotspots may be 'hotter' for genes involved in parasitic interactions post-germination than for SL perception. Kenyan *S. hermonthica* populations exhibit a more generalist germination response compared to populations from West Africa, which show pronounced differences in response to orobanchol vs. 5-deoxystrigol from host root exudates or

to strigolactone standards (Parker and Reid, 1979; Haussmann et al., 2004; Bellis et al., 2020). This idea also corresponds with previous findings that East African *S. hermonthica* may have greater average infestation success across diverse sorghum genotypes than West African populations (Bozkurt et al., 2015). Functional G_H x G_P in strigolactone response variation may segregate among populations in a different part of the parasite range than studied here, for example among West African populations, or at a broader spatial scale, for example in West vs. East African parasite populations (Haussmann et al., 2004; Bellis et al., 2020).

In contrast to general expectations (Nuismer and Dybdahl, 2016), our genomic analyses revealed the strongest evidence for host-specific selection on genes involved in the later stages of parasite development (Fig. 3, Fig. S3). The best evidence for host-specific selection on haustorium loci came from our analyses of a transcript annotated as a chemocyanin precursor (Fig. 3). In addition to strong differentiation between finger millet and maize hosts, the 1-kb region including the chemocyanin exhibited an excess of rare polymorphism and multiple alleles (Fig. S4-5), consistent with expectations for recurrent soft sweeps from standing genetic variation (Pennings and Hermisson, 2006). Notably, even the strongest signals of host-specific selection detected in our study did not reveal any loci exhibiting complete differentiation between parasites on different hosts, indicating that there may be relatively few genetic barriers to parasitism of different cereal host species in our region. The ‘finger millet’ chemocyanin allele, for example, was also present at low frequency in the genomes of parasites on other host species. This suggests a neutral impact of the allele on parasitism of other hosts, given that all sequenced parasite individuals were already at an advanced life stage. The importance of conditional neutrality for local adaptation in other systems (Lowry et al., 2019) further highlights the complexity of selective pressures shaping local adaptation of parasitic plants to dynamic host communities.

CONCLUSIONS

While our results emphasize the challenges of *Striga* management due to high genomic diversity and adaptive potential, they also highlight the promise of low coverage WGS approaches for functional genomics of non-model species. The outlier signal for two of the three candidate loci we describe in detail here resulted from structural variation that would not have been uncovered in an alignment-based analysis or using a RAD-Seq approach that may only survey a small portion of the genome or be prone to allele drop-out. Reference-free approaches continue to gain ground for studies of genomic and phenotypic variation in plants, with well-documented advantages (VanWallendael and Alvarez, 2020; Voichek and Weigel, 2020). Our study indicates that the utility of large WGS datasets may not be out of reach even for species such as *Striga hermonthica* characterized by large, complex genomes. As the need to mitigate biotic constraints on global food security becomes increasingly critical, reference-free analyses coupled with WGS data may serve as a promising strategy for rapid characterization of alleles involved in parasite adaptation across diverse environments.

ACKNOWLEDGMENTS

This study is based on work supported by a National Science Foundation Postdoctoral Research Fellowship in Biology to E.S.B. under Grant 1711950, the Arkansas Biosciences Institute (the major research component of the Arkansas Tobacco Settlement Proceeds Act of 2000), and the *Emmy Noether*-program of the German Science Foundation (WI4507/3-1 to S.W.). A.K. and X.H. were supported by NSF EPSCoR Award 1946391. J.R.L. was supported by NIH 1 R35 GM138300-01.

AUTHOR CONTRIBUTIONS

C.S.v.M., S.W., C.O.O., E.K., T.X., and E.S.B collected and processed samples and performed laboratory experiments. C.S.v.M., S.W., A.K., and E.S.B. carried out analyses. X.H., S.W.,

S.M.R., C.W.D., J.R.L., and E.S.B. contributed to experimental design and interpretation. E.S.B. and J.R.L. drafted the manuscript, with input and critical revision from all authors. All authors approved the final version of the manuscript.

DATA AND CODE AVAILABILITY

Raw reads from whole genome sequencing of the 68 *S. hermonthica* individuals from the 2018 collection and the Ugandan reference have been deposited in the National Center for Biotechnology Information (NCBI) Sequence Read Archive (SRA) database, https://www.ncbi.nlm.nih.gov/sra (BioProject accession no. PRJNA801489). The reference assembly of the Ugandan specimen is available for download and BLAST searches on *WARPP* (https://warpp.app; (Kösters et al., 2021). Images associated with the different collection sites are available from iNaturalist. Germination rate data and code to reproduce the analyses are available at https://github.com/em-bellis/StrigaWGS.

SUPPLEMENTARY INFORMATION

Additional supporting information may be found online in the Supporting Information Section at the end of the article.

Appendix S1: Supplementary Figures and Tables.

LITERATURE CITED

Akiyama, K., K. Matsuzaki, and H. Hayashi. 2005. Plant sesquiterpenes induce hyphal branching in arbuscular mycorrhizal fungi. *Nature* 435: 824–827.

Awad, A. A., D. Sato, D. Kusumoto, H. Kamioka, Y. Takeuchi, and K. Yoneyama. 2006. Characterization of Strigolactones, Germination Stimulants for the Root Parasitic Plants

572 *Striga* and *Orobanche*, Produced by Maize, Millet and Sorghum. *Plant Growth*
573 *Regulation* 48: 221.

574 Bankevich, A., S. Nurk, D. Antipov, A. A. Gurevich, M. Dvorkin, A. S. Kulikov, V. M. Lesin, et al.
575 2012. SPAdes: a new genome assembly algorithm and its applications to single-cell
576 sequencing. *Journal of computational biology* 19: 455–477.

577 Bates, D., M. Mächler, B. Bolker, and S. Walker. 2015. Fitting Linear Mixed-Effects Models
578 Using lme4. *Journal of Statistical Software* 67: 1–48.

579 Baucom, R. S. 2019. Evolutionary and ecological insights from herbicide-resistant weeds: what
580 have we learned about plant adaptation, and what is left to uncover? *New Phytologist*
581 223: 68–82.

582 Bebawi, F. F., R. E. Eplee, C. E. Harris, and R. S. Norris. 1984. Longevity of witchweed (*Striga*
583 *asiatica*) seed. *Weed Science* 32: 494–497.

584 Bellis, E., and E. Kelly. 2019. *Striga hermonthica* germination assay. *protocols.io*.

585 Bellis, E. S., E. A. Kelly, C. M. Lorts, H. Gao, V. L. DeLeo, G. Rouhan, A. Budden, et al. 2020.
586 Genomics of sorghum local adaptation to a parasitic plant. *Proceedings of the National*
587 *Academy of Sciences* 117: 4243.

588 Bellis, E. S., C. M. McLaughlin, C. W. dePamphilis, and J. R. Lasky. 2021. The geography of
589 parasite local adaptation to host communities. *Ecography*.

590 Bolger, A. M., M. Lohse, and B. Usadel. 2014. Trimmomatic: a flexible trimmer for Illumina
591 sequence data. *Bioinformatics* 30: 2114–2120.

592 Bolnick, D. I., L. H. Yang, J. A. Fordyce, J. M. Davis, and R. Svanbäck. 2002. Measuring
593 Individual-Level Resource Specialization. *Ecology* 83: 2936–2941.

594 Bozkurt, M. L., P. Muth, H. K. Parzies, and B. I. G. Haussmann. 2015. Genetic diversity of East
595 and West African *Striga hermonthica* populations and virulence effects on a contrasting
596 set of sorghum cultivars. *Weed Research* 55: 71–81.

597 Bushnell, B. BBMap. Website sourceforge.net/projects/bbmap/.

598 Cardoso, C., T. Charnikhova, M. Jamil, P.-M. Delaux, F. Verstappen, M. Amini, D.
599 Lauressergues, et al. 2014. Differential Activity of *Striga hermonthica* Seed Germination
600 Stimulants and *Gigaspora rosea* Hyphal Branching Factors in Rice and Their
601 Contribution to Underground Communication. *PLOS ONE* 9: 1–11.

602 Castellano, D., L. H. Uricchio, K. Munch, and D. Enard. 2019. Viruses rule over adaptation in
603 conserved human proteins. *bioRxiv*: 555060.

604 Charnikhova, T. V., K. Gaus, A. Lumbroso, M. Sanders, J.-P. Vincken, A. D. Mesmaeker, C. P.
605 Ruyter-Spira, et al. 2017. Zealactones. Novel natural strigolactones from maize.
606 *Phytochemistry* 137: 123–131.

607 Conn, C. E., R. Bythell-Douglas, D. Neumann, S. Yoshida, B. Whittington, J. H. Westwood, K.
608 Shirasu, et al. 2015. Convergent evolution of strigolactone perception enabled host
609 detection in parasitic plants. *Science* 349: 540–543.

610 Cui, S., S. Wada, Y. Tobimatsu, Y. Takeda, S. B. Saucet, T. Takano, T. Umezawa, et al. 2018.
611 Host lignin composition affects haustorium induction in the parasitic plants
612 *Phtheirospermum japonicum* and *Striga hermonthica*. *New Phytologist* 218: 710–723.

613 Dayou, O., W. Kibet, P. Ojola, P. I. Gangashetty, S. Wicke, and S. Runo. 2021. Two-tier
614 witchweed (*Striga hermonthica*) resistance in wild pearl millet (*Pennisetum glaucum*)
615 29Aw. *Weed Science* 69: 300–306.

616 Ebert, D., and P. D. Fields. 2020. Host–parasite co-evolution and its genomic signature. *Nature*
617 *Reviews Genetics* 21: 754–768.

618 Ejeta, G. 2007. The Striga scourge in Africa: a growing pandemic. Integrating new technologies
619 for Striga control: towards ending the witch-hunt, 3–16. World Scientific.

620 Estep, M. C., B. S. Gowda, K. Huang, M. P. Timko, and J. L. Bennetzen. 2012. Genomic
621 characterization for parasitic weeds of the genus *Striga* by sample sequence analysis.
622 *The Plant Genome* 5.

623 Fumagalli, M., M. Sironi, U. Pozzoli, A. Ferrer-Admettla, L. Pattini, and R. Nielsen. 2011.
624 Signatures of environmental genetic adaptation pinpoint pathogens as the main selective
625 pressure through human evolution. *PLoS genetics* 7: e1002355.

626 Gbèhounou, G., A. H. Pieterse, and J. A. Verkleij. 2003. Longevity of Striga seeds reconsidered:
627 results of a field study on purple witchweed (*Striga hermonthica*) in Benin. *Weed*
628 *Science* 51: 940–946.

629 Gethi, J. G., M. E. Smith, S. E. Mitchell, and S. Kresovich. 2005. Genetic diversity of *Striga*
630 *hermonthica* and *Striga asiatica* populations in Kenya. *Weed Research* 45: 64–73.

631 Gobena, D., M. Shimels, P. J. Rich, C. Ruyter-Spira, H. Bouwmeester, S. Kanuganti, T.
632 Mengiste, and G. Ejeta. 2017. Mutation in sorghum LOW GERMINATION STIMULANT 1
633 alters strigolactones and causes *Striga* resistance. *Proceedings of the National*
634 *Academy of Sciences* 114: 4471–4476.

635 Gurevich, A., V. Saveliev, N. Vyahhi, and G. Tesler. 2013. QUAST: quality assessment tool for
636 genome assemblies. *Bioinformatics* 29: 1072–1075.

637 Hall, M. D., G. Bento, and D. Ebert. 2017. The evolutionary consequences of stepwise infection
638 processes. *Trends in Ecology & Evolution* 32: 612–623.

639 Hall, M. D., J. Routtu, and D. Ebert. 2019. Dissecting the genetic architecture of a stepwise
640 infection process. *Molecular ecology* 28: 3942–3957.

641 Haussmann, B., D. Hess, G. Omanya, R. Folkertsma, B. Reddy, M. Kayentao, H. Welz, and H.
642 Geiger. 2004. Genomic regions influencing resistance to the parasitic weed *Striga*
643 *hermonthica* in two recombinant inbred populations of sorghum. *Theoretical and Applied*
644 *Genetics* 109: 1005–1016.

645 Honaas, L. A., E. K. Wafula, Z. Yang, J. P. Der, N. J. Wickett, N. S. Altman, C. G. Taylor, et al.
646 2013. Functional genomics of a generalist parasitic plant: Laser microdissection of host-
647 parasite interface reveals host-specific patterns of parasite gene expression. *BMC Plant*
648 *Biology* 13: 9.

649 Ichihashi, Y., M. Kusano, M. Kobayashi, K. Suetsugu, S. Yoshida, T. Wakatake, K. Kumaishi, et
650 al. 2017. Transcriptomic and Metabolomic Reprogramming from Roots to Haustoria in
651 the Parasitic Plant, *Thesium chinense*. *Plant and Cell Physiology* 59: 729–738.

652 Jackman, S. D., B. P. Vandervalk, H. Mohamadi, J. Chu, S. Yeo, S. A. Hammond, G. Jahesh, et
653 al. 2017. ABySS 2.0: resource-efficient assembly of large genomes using a Bloom filter.
654 *Genome research* 27: 768–777.

655 Kavuluko, J., M. Kibe, I. Sugut, W. Kibet, J. Masanga, S. Mutinda, M. Wamalwa, et al. 2020.
656 GWAS provides biological insights into mechanisms of the parasitic plant (*Striga*)
657 resistance in Sorghum.

658 Kim, G., M. L. LeBlanc, E. K. Wafula, C. W. DePamphilis, and J. H. Westwood. 2014. Genomic-
659 scale exchange of mRNA between a parasitic plant and its hosts. *Science* 345: 808–
660 811.

661 Kim, S., J.-C. Mollet, J. Dong, K. Zhang, S.-Y. Park, and E. M. Lord. 2003. Chemocyanin, a
662 small basic protein from the lily stigma, induces pollen tube chemotropism. *Proceedings*
663 *of the National Academy of Sciences* 100: 16125–16130.

664 Kim, S. Y., K. E. Lohmueller, A. Albrechtsen, Y. Li, T. Korneliussen, G. Tian, N. Grarup, et al.
665 2011. Estimation of allele frequency and association mapping using next-generation
666 sequencing data. *BMC Bioinformatics* 12: 231.

667 Korneliussen, T. S., A. Albrechtsen, and R. Nielsen. 2014. ANGSD: Analysis of Next Generation
668 Sequencing Data. *BMC Bioinformatics* 15: 356.

669 Kösters, L. M., S. Wiechers, P. Lyko, K. F. Müller, and S. Wicke. 2021. WARPP—web
670 application for the research of parasitic plants. *Plant Physiology* 185: 1374–1380.

671 Li, H. 2013. Aligning sequence reads, clone sequences and assembly contigs with BWA-MEM.

672 Li, H., B. Handsaker, A. Wysoker, T. Fennell, J. Ruan, N. Homer, G. Marth, et al. 2009. The
673 Sequence Alignment/Map format and SAMtools. *Bioinformatics* 25: 2078–2079.

674 Li, J., and M. P. Timko. 2009. Gene-for-gene resistance in *Striga*-cowpea associations. *Science*
675 325: 1094–1094.

676 Liu, N., G. Shen, Y. Xu, H. Liu, J. Zhang, S. Li, J. Li, et al. 2020. Extensive inter-plant protein
677 transfer between *Cuscuta* parasites and their host plants. *Molecular plant* 13: 573–585.

678 Lopez, L., E. S. Bellis, E. Wafula, S. J. Hearne, L. Honaas, P. E. Ralph, M. P. Timko, et al.
679 2019. Transcriptomics of host-specific interactions in natural populations of the parasitic
680 plant purple witchweed (*Striga hermonthica*). *Weed Science* 67: 397–411.

681 Lou, R., A. Jacobs, A. Wilder, and N. O. Therkildsen. 2021. A beginner's guide to low-coverage
682 whole genome sequencing for population genomics. *Authorea*.

683 Louthan, A. M., and K. M. Kay. 2011. Comparing the adaptive landscape across trait types:
684 larger QTL effect size in traits under biotic selection. *BMC evolutionary biology* 11: 1–12.

685 Lowry, D. B., S. Hoban, J. L. Kelley, K. E. Lotterhos, L. K. Reed, M. F. Antolin, and A. Storfer.
686 2017. Breaking RAD: an evaluation of the utility of restriction site-associated DNA
687 sequencing for genome scans of adaptation. *Molecular Ecology Resources* 17: 142–
688 152.

689 Lowry, D. B., J. T. Lovell, L. Zhang, J. Bonnette, P. A. Fay, R. B. Mitchell, J. Lloyd-Reilley, et al.
690 2019. QTL × environment interactions underlie adaptive divergence in switchgrass
691 across a large latitudinal gradient. *Proceedings of the National Academy of Sciences*
692 116: 12933.

693 Lyko, P., and S. Wicke. 2021. Genomic reconfiguration in parasitic plants involves considerable
694 gene losses alongside global genome size inflation and gene births. *Plant Physiology*
695 186: 1412–1423.

696 Mallu, T. S., S. Mutinda, S. M. Githiri, D. Achieng Odeny, and S. Runo. 2021. New pre-
697 attachment *Striga* resistant sorghum adapted to African agro-ecologies. *Pest*
698 *Management Science* 77: 2894–2902.

699 Masumoto, N., Y. Suzuki, S. Cui, M. Wakazaki, M. Sato, K. Kumaishi, A. Shibata, et al. 2021.
700 Three-dimensional reconstructions of haustoria in two parasitic plant species in the
701 Orobanchaceae. *Plant Physiology* 185: 1429–1442.

702 Mbuvi, D. A., C. W. Masiga, E. K. Kuria, J. Masanga, M. Wamalwa, A. Mohamed, D. Odeny, et
703 al. 2017. Novel sources of witchweed (*Striga*) resistance from wild sorghum accessions.
704 *Frontiers in plant science* 8: 116.

705 Mutinda, S. M., J. Masanga, J. M. Mutuku, S. Runo, and A. Alakonya. 2018. KSTP 94, an open-
706 pollinated maize variety has postattachment resistance to purple witchweed (*Striga*
707 *hermonthica*). *Weed science* 66: 525–529.

708 Nei, M. 1973. Analysis of Gene Diversity in Subdivided Populations. *Proceedings of the National*
709 *Academy of Sciences* 70: 3321–3323.

710 Nei, M., and R. K. Chesser. 1983. Estimation of fixation indices and gene diversities. *Annals of*
711 *Human Genetics* 47: 253–259.

712 Nelson, D. C. 2021. The mechanism of host-induced germination in root parasitic plants. *Plant*
713 *Physiology* 185: 1353–1373.

714 Nuismer, S. L., and M. F. Dybdahl. 2016. Quantifying the coevolutionary potential of multistep
715 immune defenses. *Evolution* 70: 282–295.

716 Ondov, B. D., T. J. Treangen, P. Melsted, A. B. Mallonee, N. H. Bergman, S. Koren, and A. M.
717 Phillippy. 2016. Mash: fast genome and metagenome distance estimation using
718 MinHash. *Genome Biology* 17: 132.

719 Padgham, M., and M. D. Sumner. 2021. geodist: Fast, Dependency-Free Geodesic Distance
720 Calculations.

721 Paradis, E., and K. Schliep. 2019. ape 5.0: an environment for modern phylogenetics and
722 evolutionary analyses in R. *Bioinformatics* 35: 526–528.

723 Parker, C., and D. C. Reid. 1979. Host specificity in *Striga* species: Some preliminary
724 observations. Proceeding of the Second International Symposium on Parasitic Weeds,
725 Raleigh, NC, 1979,.

726 Pennings, P. S., and J. Hermisson. 2006. Soft sweeps III: the signature of positive selection
727 from recurrent mutation. *PLoS genetics* 2: e186.

728 Poland, J. A., P. J. Balint-Kurti, R. J. Wisser, R. C. Pratt, and R. J. Nelson. 2009. Shades of
729 gray: the world of quantitative disease resistance. *Trends in plant science* 14: 21–29.

730 R Core Team. 2020. R: A language and environment for statistical computing. R Foundation for
731 Statistical Computing, Vienna, Austria.

732 Rahman, A., I. Hallgrímsdóttir, M. Eisen, and L. Pachter. 2018. Association mapping from
733 sequencing reads using *k*-mers J. Flint [ed.],. *eLife* 7: e32920.

734 Ravensdale, M., A. Nemri, P. H. Thrall, J. G. Ellis, and P. N. Dodds. 2011. Co-evolutionary
735 interactions between host resistance and pathogen effector genes in flax rust disease.
736 *Molecular plant pathology* 12: 93–102.

737 Savary, S., L. Willocquet, S. J. Pethybridge, P. Esker, N. McRoberts, and A. Nelson. 2019. The
738 global burden of pathogens and pests on major food crops. *Nature ecology & evolution*
739 3: 430–439.

740 Shahid, S., G. Kim, N. R. Johnson, E. Wafula, F. Wang, C. Coruh, V. Bernal-Galeano, et al.
741 2018. MicroRNAs from the parasitic plant *Cuscuta campestris* target host messenger
742 RNAs. *Nature* 553: 82–85.

743 Shen, G., N. Liu, J. Zhang, Y. Xu, I. T. Baldwin, and J. Wu. 2020. *Cuscuta australis* (dodder)
744 parasite eavesdrops on the host plants' FT signals to flower. *Proceedings of the National*
745 *Academy of Sciences* 117: 23125–23130.

746 Spallek, T., M. Mutuku, and K. Shirasu. 2013. The genus *Striga*: a witch profile. *Molecular plant*
747 *pathology* 14: 861–869.

748 Therkildsen, N. O., and S. R. Palumbi. 2017. Practical low-coverage genome-wide sequencing
749 of hundreds of individually barcoded samples for population and evolutionary genomics
750 in nonmodel species. *Molecular Ecology Resources* 17: 194–208.

751 Thompson, J. N. 2005. The geographic mosaic of coevolution. University of Chicago Press.

752 Thrall, P. H., A.-L. Laine, M. Ravensdale, A. Nemri, P. N. Dodds, L. G. Barrett, and J. J. Burdon.
753 2012. Rapid genetic change underpins antagonistic coevolution in a natural host-
754 pathogen metapopulation. *Ecology letters* 15: 425–435.

755 Timko, M. P., K. Huang, and K. E. Lis. 2012. Host resistance and parasite virulence in *Striga*–
756 host plant interactions: A shifting balance of power. *Weed Science* 60: 307–315.

757 Toh, S., D. Holbrook-Smith, P. J. Stogios, O. Onopriyenko, S. Lumba, Y. Tsuchiya, A.
758 Savchenko, and P. McCourt. 2015. Structure-function analysis identifies highly sensitive
759 strigolactone receptors in *Striga*. *Science* 350: 203–207.

760 Tsuchiya, Y., M. Yoshimura, Y. Sato, K. Kuwata, S. Toh, D. Holbrook-Smith, H. Zhang, et al.
761 2015. Probing strigolactone receptors in *Striga hermonthica* with fluorescence. *Science*
762 349: 864–868.

763 Unachukwu, N. N., A. Menkir, I. Y. Rabbi, M. Oluoch, S. Muranaka, A. Elzein, G. Odhiambo, et
764 al. 2017. Genetic diversity and population structure of *Striga hermonthica* populations
765 from Kenya and Nigeria. *Weed Research* 57: 293–302.

766 VanWallendael, A., and M. Alvarez. 2020. Alignment-free methods for polyploid genomes: quick
767 and reliable genetic distance estimation. *bioRxiv*.

768 Vigueira, C. C., K. M. Olsen, and A. L. Caicedo. 2013. The red queen in the corn: agricultural
769 weeds as models of rapid adaptive evolution. *Heredity* 110: 303—311.

770 Voichek, Y., and D. Weigel. 2020. Identifying genetic variants underlying phenotypic variation in
771 plants without complete genomes. *Nature Genetics* 52: 534–540.

772 Westwood, J. H., C. W. dePamphilis, M. Das, M. Fernández-Aparicio, L. A. Honaas, M. P.
773 Timko, E. K. Wafula, et al. 2012. The Parasitic Plant Genome Project: New Tools for
774 Understanding the Biology of Orobanche and Striga. *Weed Science* 60: 295–306.

775 Wicke, S., K. F. Müller, C. W. dePamphilis, D. Quandt, S. Bellot, and G. M. Schneeweiss. 2016.
776 Mechanistic model of evolutionary rate variation en route to a nonphotosynthetic lifestyle
777 in plants. *Proceedings of the National Academy of Sciences* 113: 9045–9050.

778 Wicke, S., K. F. Müller, C. W. de Pamphilis, D. Quandt, N. J. Wickett, Y. Zhang, S. S. Renner,
779 and G. M. Schneeweiss. 2013. Mechanisms of functional and physical genome
780 reduction in photosynthetic and nonphotosynthetic parasitic plants of the broomrape
781 family. *The Plant Cell* 25: 3711–3725.

782 Wilfert, L., and P. Schmid-Hempel. 2008. The genetic architecture of susceptibility to parasites.
783 *BMC Evolutionary Biology* 8: 1–8.

784 Wood, D. E., J. Lu, and B. Langmead. 2019. Improved metagenomic analysis with Kraken 2.
785 *Genome biology* 20: 1–13.

786 Yang, Z., E. K. Wafula, L. A. Honaas, H. Zhang, M. Das, M. Fernandez-Aparicio, K. Huang, et
787 al. 2014. Comparative Transcriptome Analyses Reveal Core Parasitism Genes and
788 Suggest Gene Duplication and Repurposing as Sources of Structural Novelty. *Molecular*
789 *Biology and Evolution* 32: 767–790.

790 Yang, Z., E. K. Wafula, G. Kim, S. Shahid, J. R. McNeal, P. E. Ralph, P. R. Timilsena, et al.
791 2019. Convergent horizontal gene transfer and cross-talk of mobile nucleic acids in
792 parasitic plants. *Nature Plants* 5: 991–1001.

793 Yoneyama, K., R. Arakawa, K. Ishimoto, H. I. Kim, T. Kisugi, X. Xie, T. Nomura, et al. 2015.
794 Difference in *Striga*-susceptibility is reflected in strigolactone secretion profile, but not in
795 compatibility and host preference in arbuscular mycorrhizal symbiosis in two maize
796 cultivars. *New Phytologist* 206: 983–989.

797 Yoneyama, K., X. Xie, H. Sekimoto, Y. Takeuchi, S. Ogasawara, K. Akiyama, H. Hayashi, and
798 K. Yoneyama. 2008. Strigolactones, host recognition signals for root parasitic plants and
799 arbuscular mycorrhizal fungi, from Fabaceae plants. *New Phytologist* 179: 484–494.

800 Yoshida, S., J. K. Ishida, N. M. Kamal, A. M. Ali, S. Namba, and K. Shirasu. 2010. A full-length
801 enriched cDNA library and expressed sequence tag analysis of the parasitic weed,
802 *Striga hermonthica*. *BMC Plant Biology* 10: 1–10.

803 Yoshida, S., S. Kim, E. K. Wafula, J. Tanskanen, Y.-M. Kim, L. Honaas, Z. Yang, et al. 2019.
804 Genome sequence of *Striga asiatica* provides insight into the evolution of plant
805 parasitism. *Current Biology* 29: 3041–3052.

806

807

Appendix S1: Supplementary Figures and Tables

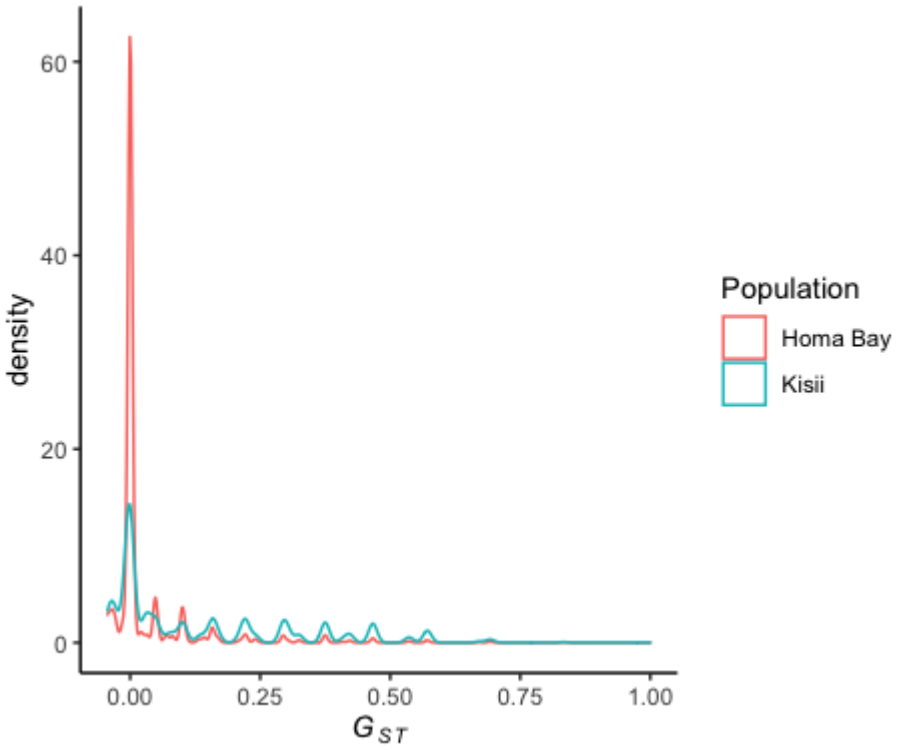

Figure S1. Distribution of G_{ST} *values.* For Homa Bay, G_{ST} is based on comparisons for parasites on adjacent plots of maize vs. sorghum at 2,765,562 *31*-mers. For Kisii, G_{ST} is based on comparisons for parasites on adjacent plots of maize vs. sorghum at 2,123,902 *31*-mers.

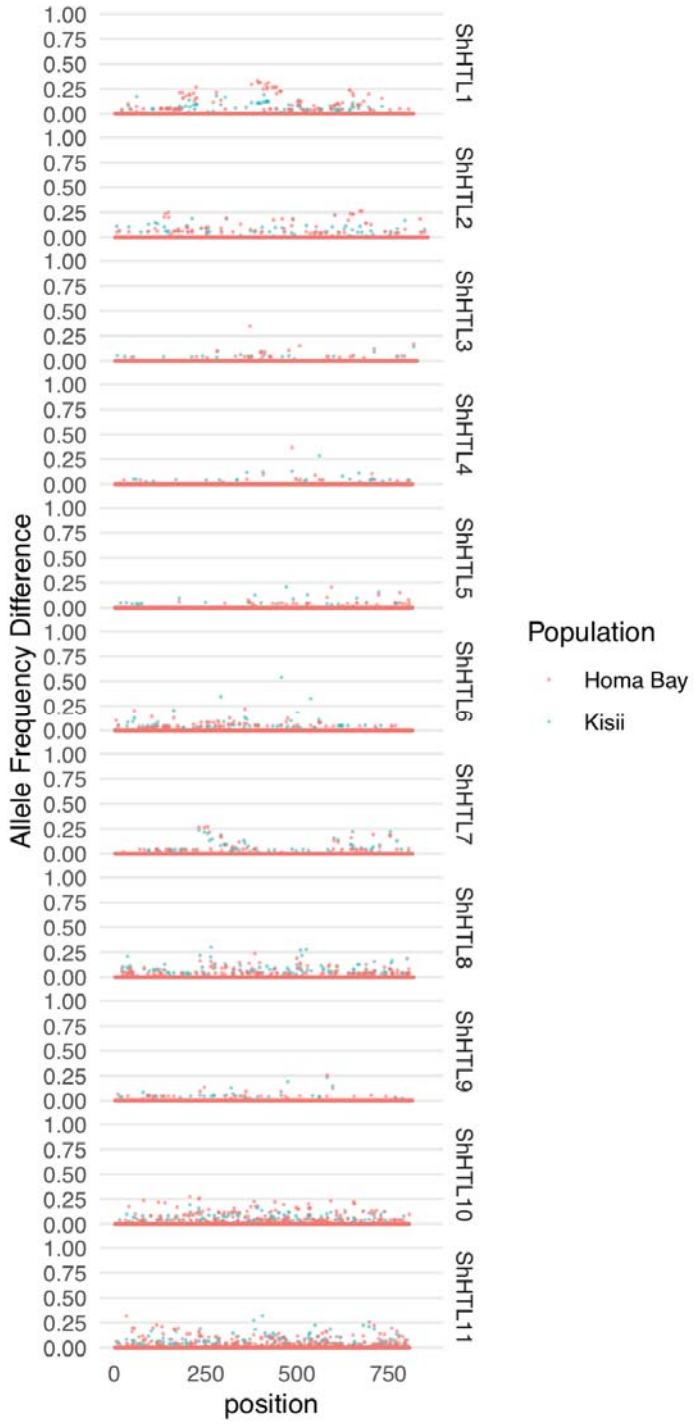

816

817

818 **Figure S2.** Allele frequency differences for 11 *ShHTL* receptors from Tsuchiya et al. (2015).

819 Allele frequencies were estimated from genotype likelihoods based on reads mapped to each

820 reference transcript. Allele frequency was estimated for parasites on each host species

821 separately (*n* = 12 per unique host and population). The difference in allele frequency estimates
822 between two hosts within a single population is shown.
823

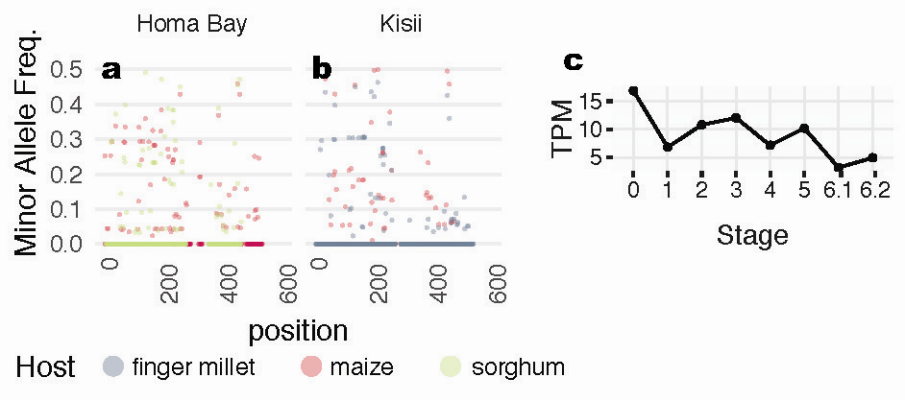

824

825 **Figure S3.** (a,b) Minor allele frequency differences based on alignments to the *SGT1* transcript
826 sequence (StHeBC4_p_c12587_g2_i1), split by population. If the locus is not present in any of
827 the sequenced individuals for that population due to genetic structural variation, no data point is
828 shown. Frequencies were estimated based on genotype likelihoods from *n* = 12 individuals per
829 unique host and population. (c) Gene expression data in transcripts per million (TPM) from the
830 PPGPII data across the 6 stages of haustorial development from data published.
831

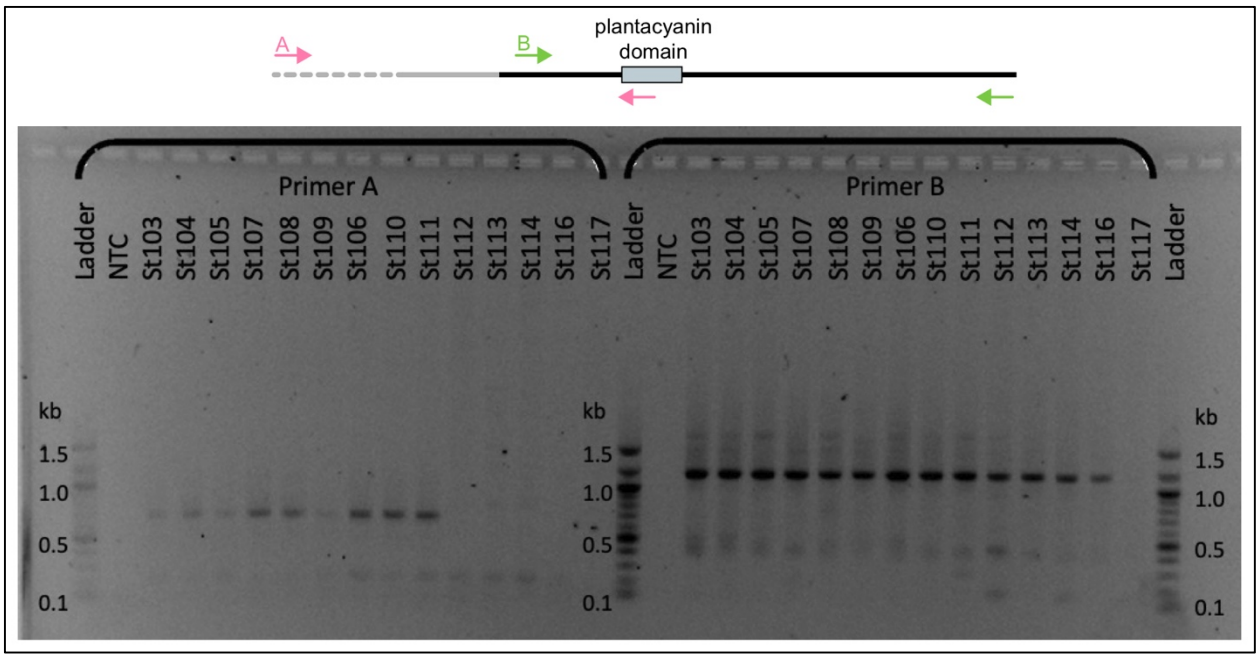

Figure S4. PCR banding results to confirm chemocyanin deletion calls. In the top panel, binding sites for primer sets A (pink) and B (green) are shown relative to location of the transcript sequence (solid black line), location of the deletion (grey dashed line), and conserved plantacyanin domain (light blue rectangle). Primer set A does not yield a 676-bp band for individuals with the deletion (lanes 11-15) whereas primer set B amplifies a region downstream of the deletion. NTC: no template control.

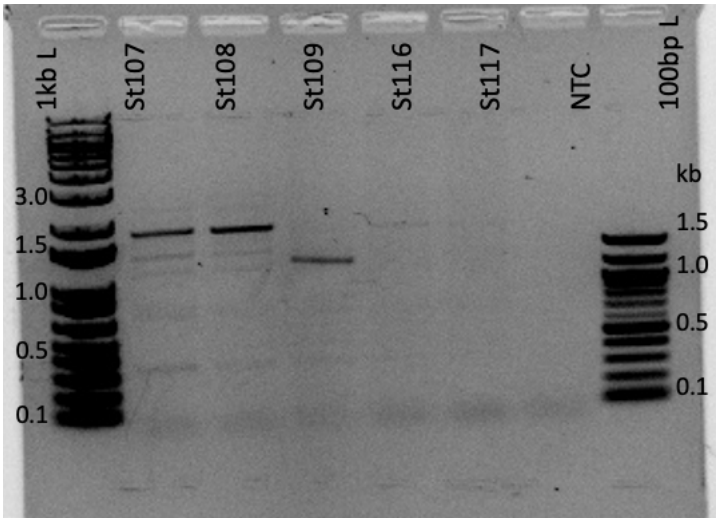

Figure S5. PCR banding results suggest multiple deletion variants. PCR amplification using the outer primers from set A (5'-TCTCGATCCTTTTGGAATGG-3') and B (5'-TGGGGAAAGAGGTAGTGCAA-3'); see Fig. S4). NTC: no template control. Lane 1: Sh107; Lane 2: Sh108, Lane 3: Sh109; Lane 4: Sh116; Lane 5: Sh117.

847 **Table S1.** GLMM for analysis of germination rate variation

	Estimate	**Std. Error**	**z-value**	***P***
Intercept	2.29	0.97	2.37	0.017
Site == Kisii	-2.16	0.79	-2.72	0.006
Host == Maize	-1.13	0.79	-1.43	0.153
Host == Sorghum	-1.90	1.12	-1.70	0.089
Treatment == ORO	-0.16	0.06	-2.85	0.004

848

849

850

851 **Table S2.** Hits to transcripts from the Parasitic Plant Genome Project (PPGPII) or Sh14v2 (from
852 Yoshida 2019) for contigs assembled from host-associated *k*-mers for *Striga hermontica* Homa
853 Bay population (maize vs. sorghum hosts). Transcripts with greater than 85% identity over at
854 least 45 bp are shown.

PGPPII	Sh14v2	Description
StHeBC4_p_c26811_g0_i3	Sh14Contig_5850	lipid-a-disaccharide synthase-like
None	Sh14Contig_37747	None
None	Sh14Contig_44696	None
StHeBC4_p_c12903_g35328_i2	Sh14Contig_229	retrotransposon gag protein
StHeBC4_p_c12587_g2_i1	Sh14Contig_28742	disease-resistance protein SGT1
None	Sh14Contig_5301	None
None	Sh14Contig_37747	None
None	Sh14Contig_60980	hypothetical protein ASPNIDRAFT_144168
StHeBC4_u_c25350_g11_i1	Sh14Contig_78939	None
None	Sh14Contig_41198	None
None	Sh14Contig_32559	None
StHeBC4_u_c12903_g30818_i7	Sh14Contig_35967	None
None	Sh14Contig_47805	None
StHeBC4_p_c9824_g0_i1	None	None
StHeBC4_p_c12903_g42998_i1	None	None

855

Table S3. Hits to transcripts from the Parasitic Plant Genome Project (PPGPII) or Sh14v2 (from Yoshida 2019) for contigs assembled from host-associated *k*-mers for *Striga hermontica* Kisii population (maize vs. finger millet hosts). Transcripts with greater than 85% identity over at least 45 bp are shown.

PGPPII	Sh14v2	Description
None	Sh14Contig_45649	None
StHeBC4_u_c12903_g32907_i4	Sh14Contig_20178	probable nicotinate-nucleotide pyrophosphorylase
StHeBC4_u_c12903_g22013_i6	Sh14Contig_24947	None
StHeBC4_u_c3941_g0_i1	Sh14Contig_42609	hypothetical protein VITISV_012016
None	Sh14Contig_70490	None
StHeBC4_u_c12903_g34431_i1	Sh14Contig_17925	upf0326 protein at4g17486-like
StHeBC4_p_c12903_g35474_i1	Sh14Contig_4481	None
StHeBC4_u_c24490_g2_i1	Sh14Contig_81114	None
StHeBC4_p_c12903_g14638_i24	Sh14Contig_23122	far-red impaired response protein
StHeBC4_u_c12903_g34431_i2	Sh14Contig_17925	upf0326 protein at4g17486-like
StHeBC4_u_c12903_g19156_i3	Sh14Contig_3012	alcohol dehydrogenase homolog
StHeBC4_p_c26043_g0_i2	Sh14Contig_13886	omega-amidase nit2
StHeBC4_p_c12903_g10585_i1	Sh14Contig_34611	None
None	Sh14Contig_20326	None
StHeBC4_p_c12903_g6756_i1	Sh14Contig_12790	None
StHeBC4_u_c12903_g15860_i5	Sh14Contig_29096	None
StHeBC4_u_c12903_g7220_i1	Sh14Contig_60050	None
None	Sh14Contig_3989	None
StHeBC4_p_c12903_g2276_i2	Sh14Contig_4881	rna polymerase ii c-terminal domain phosphatase-like 1-like
StHeBC4_u_c12903_g1840_i3	Sh14Contig_19406	e3 ubiquitin-protein ligase ring1-like
None	Sh14Contig_71030	None
StHeBC4_p_c12903_g39698_i9	Sh14Contig_45458	gag-protease polyprotein
StHeBC4_u_c12903_g32907_i12	Sh14Contig_81511	None
StHeBC4_u_c12903_g34427_i1	Sh14Contig_46360	None
StHeBC4_p_c12903_g35474_i1	Sh14Contig_4481	None
StHeBC4_p_c12903_g11444_i1	Sh14Contig_40193	polyprotein
StHeBC4_u_c19051_g0_i1	Sh14Contig_66323	None
StHeBC4_p_c12903_g10585_i1	Sh14Contig_12790	None
StHeBC4_u_c12903_g1736_i4	Sh14Contig_28260	None
None	Sh14Contig_31117	PREDICTED: uncharacterized protein LOC100256114
StHeBC4_u_c12903_g33489_i1	Sh14Contig_51019	None
StHeBC4_p_c16693_g0_i2	Sh14Contig_33691	hypothetical protein VITISV_018984
StHeBC4_p_c23323_g2_i3	Sh14Contig_3290	diphthamide biosynthesis protein 2-like
StHeBC4_p_c18975_g7_i10	Sh14Contig_7369	None
StHeBC4_p_c12903_g4626_i6	Sh14Contig_4698	retrotransposon protein
None	Sh14Contig_80867	None
StHeBC4_h_c11261_g0_i2	Sh14Contig_13520	chemocyanin precursor
StHeBC4_p_c23585_g1_i4	Sh14Contig_1911	None
StHeBC4_p_c24979_g0_i1	Sh14Contig_4792	97 kda heat shock protein
StHeBC4_h_c12903_g23955_i1	Sh14Contig_45458	gag-protease polyprotein

StHeBC4_u_c12903_g1547_i1	Sh14Contig_68469	None
None	Sh14Contig_48379	None
StHeBC4_p_c12903_g30160_i1	Sh14Contig_57886	None
None	Sh14Contig_64011	None
None	Sh14Contig_1642	retrotransposon ty1-copia subclass
StHeBC4_p_c22011_g3_i2	Sh14Contig_15531	wd repeat-containing protein 26-like
StHeBC4_p_c12903_g7195_i9	Sh14Contig_60490	unnamed protein product
StHeBC4_h_c24484_g1_i2	Sh14Contig_42033	hypothetical protein VITISV_042364
StHeBC4_p_c20621_g7_i3	Sh14Contig_4748	gag-pol precursor
StHeBC4_u_c12903_g27039_i4	Sh14Contig_4713	pectin methylesterase
StHeBC4_p_c18975_g7_i5	Sh14Contig_7369	None
None	Sh14Contig_65419	None
StHeBC4_u_c12903_g32907_i15	Sh14Contig_29096	None
None	Sh14Contig_52781	None
StHeBC4_p_c12903_g208_i2	Sh14Contig_7920	None
StHeBC4_p_c12903_g22741_i4	Sh14Contig_9532	pattern formation
StHeBC4_p_c12903_g38175_i2	Sh14Contig_17588	ring zinc finger ankyrin protein
None	Sh14Contig_4395	unnamed protein product [Vitis vinifera]
StHeBC4_u_c12903_g34427_i3	Sh14Contig_46360	None
StHeBC4_h_c11261_g0_i1	Sh14Contig_13520	chemocyanin precursor
StHeBC4_h_c12903_g40212_i2	Sh14Contig_24771	copia ltr rider
StHeBC4_p_c13584_g0_i1	Sh14Contig_33358	None
StHeBC4_u_c12903_g16409_i3	Sh14Contig_576	atp-dependent helicase brm-like
StHeBC4_h_c11483_g0_i1	Sh14Contig_55439	FAR1; Zinc finger, SWIM-type
StHeBC4_p_c12903_g20722_i11	Sh14Contig_28640	PREDICTED: uncharacterized protein LOC100854178, partial
StHeBC4_h_c12903_g12703_i2	Sh14Contig_9184	photosystem ii cp43 chlorophyll apoprotein
StHeBC4_p_c12903_g2185_i1	Sh14Contig_12790	None
StHeBC4_p_c12903_g34644_i1	Sh14Contig_4585	trehalose-phosphatase synthase 2
StHeBC4_p_c24106_g0_i1	Sh14Contig_40210	None
StHeBC4_h_c18968_g1_i5	Sh14Contig_1642	retrotransposon ty1-copia subclass
StHeBC4_u_c3088_g0_i1	Sh14Contig_31622	None
StHeBC4_u_c12903_g35782_i1	Sh14Contig_27773	None
None	Sh14Contig_23637	None
StHeBC4_u_c19051_g0_i1	Sh14Contig_63267	None
None	Sh14Contig_11046	uncharacterized protein loc100253271
StHeBC4_u_c12903_g27691_i1	Sh14Contig_35466	None
StHeBC4_u_c22214_g0_i6	Sh14Contig_43769	None
StHeBC4_u_c12903_g1736_i12	Sh14Contig_28260	None
None	Sh14Contig_58406	None
StHeBC4_u_c26755_g1_i1	Sh14Contig_68980	None
StHeBC4_p_c26987_g0_i1	Sh14Contig_48	6-4 photolyase
StHeBC4_u_c16917_g1_i1	Sh14Contig_50405	None
StHeBC4_u_c22344_g0_i6	Sh14Contig_813	thaumatin-like protein
StHeBC4_u_c12903_g699_i2	Sh14Contig_58790	None
StHeBC4_p_c12903_g14484_i1	Sh14Contig_12513	None
StHeBC4_p_c9911_g3_i3	Sh14Contig_54171	predicted protein
None	Sh14Contig_7920	None
StHeBC4_u_c12903_g34427_i8	Sh14Contig_46360	None

StHeBC4_p_c12903_g35474_i1	Sh14Contig_4481	None
None	Sh14Contig_43642	None
StHeBC4_u_c12903_g15888_i3	Sh14Contig_81511	None
StHeBC4_p_c24979_g1_i1	Sh14Contig_4792	97 kda heat shock protein
StHeBC4_p_c12903_g14483_i5	Sh14Contig_16250	tcp transcription factor 13
StHeBC4_p_c12903_g6756_i1	Sh14Contig_12790	None
StHeBC4_p_c12903_g10875_i1	Sh14Contig_20081	beta-glucan-binding protein
StHeBC4_p_c17648_g0_i3	Sh14Contig_15582	e3 ubiquitin-protein ligase upl3
StHeBC4_u_c12903_g22225_i1	Sh14Contig_48959	None
None	Sh14Contig_45784	None
None	Sh14Contig_75797	None
StHeBC4_u_c12903_g11727_i4	Sh14Contig_4041	None
StHeBC4_p_c23083_g3_i1	Sh14Contig_37240	None
None	Sh14Contig_5997	None
None	Sh14Contig_67788	None
StHeBC4_p_c12903_g6756_i1	Sh14Contig_1062	None
StHeBC4_u_c12903_g11833_i1	Sh14Contig_14842	None
StHeBC4_p_c12903_g6700_i3	Sh14Contig_43681	hypothetical protein VITISV_013115
StHeBC4_p_c20608_g0_i7	Sh14Contig_35726	PREDICTED: putative kinase-like protein TMKL1-like
None	Sh14Contig_29426	None
None	Sh14Contig_70066	None
StHeBC4_u_c12903_g29964_i1	Sh14Contig_37086	None
StHeBC4_p_c12903_g39295_i4	Sh14Contig_19126	epoxide hydrolase 2-like
StHeBC4_u_c12903_g1736_i13	Sh14Contig_29803	None
None	Sh14Contig_29803	None
StHeBC4_p_c12903_g6843_i1	Sh14Contig_4375	translation initiation factor eif-2b subunit delta-like
StHeBC4_u_c12903_g1736_i7	Sh14Contig_28260	None
StHeBC4_p_c12903_g38577_i4	Sh14Contig_21342	None
StHeBC4_p_c25304_g0_i1	Sh14Contig_5367	serine threonine-protein kinase pbs1-like
StHeBC4_u_c12903_g1736_i12	Sh14Contig_28260	None
StHeBC4_p_c12903_g7992_i1	Sh14Contig_22515	poly-specific ribonuclease parn
StHeBC4_u_c12903_g4208_i1	Sh14Contig_47575	None
StHeBC4_p_c11471_g0_i1	Sh14Contig_66224	None
StHeBC4_p_c12903_g40108_i1	Sh14Contig_17925	upf0326 protein at4g17486-like
StHeBC4_p_c26825_g3_i2	Sh14Contig_30816	unnamed protein product
StHeBC4_u_c17841_g0_i1	Sh14Contig_54135	None
StHeBC4_h_c12903_g30936_i1	Sh14Contig_28702	copia LTR rider
None	Sh14Contig_37720	None
StHeBC4_p_c12903_g10585_i1	Sh14Contig_12790	None
StHeBC4_u_c14956_g0_i2	Sh14Contig_3380	None
StHeBC4_u_c12903_g19836_i1	Sh14Contig_44128	None
StHeBC4_p_c12903_g9452_i3	Sh14Contig_68177	None
StHeBC4_p_c21038_g1_i1	Sh14Contig_46012	None
StHeBC4_u_c12903_g35474_i11	Sh14Contig_4481	None
StHeBC4_p_c12903_g15810_i1	Sh14Contig_12790	None
StHeBC4_u_c12903_g1736_i7	Sh14Contig_28260	None
StHeBC4_u_c12903_g34427_i1	Sh14Contig_61194	None

StHeBC4_p_c18569_g2_i14	Sh14Contig_67725	None
StHeBC4_u_c22214_g0_i2	Sh14Contig_43769	None
StHeBC4_p_c18975_g4_i3	Sh14Contig_77966	hypothetical protein VITISV_037041
StHeBC4_p_c22472_g0_i1	Sh14Contig_63886	predicted protein
StHeBC4_u_c24133_g4_i1	Sh14Contig_30270	None
StHeBC4_u_c12903_g12274_i1	Sh14Contig_5997	None
None	Sh14Contig_267	None
StHeBC4_u_c12903_g34427_i3	Sh14Contig_31554	None
StHeBC4_p_c12903_g33372_i2	Sh14Contig_18809	serine threonine protein kinase
StHeBC4_p_c12903_g12842_i2	Sh14Contig_58393	hypothetical protein VITISV_012059
StHeBC4_p_c12903_g13577_i4	Sh14Contig_4336	retrotransposon unclassified
StHeBC4_u_c12903_g34427_i9	Sh14Contig_46360	None
StHeBC4_u_c20739_g0_i7	Sh14Contig_30629	None
None	Sh14Contig_64863	None
StHeBC4_u_c18975_g2_i1	Sh14Contig_7369	None
StHeBC4_u_c3227_g1_i1	Sh14Contig_65419	None
StHeBC4_u_c18360_g0_i1	Sh14Contig_44903	None
StHeBC4_p_c12903_g6756_i1	Sh14Contig_1062	None
StHeBC4_p_c12903_g20268_i2	Sh14Contig_73193	None
StHeBC4_p_c12903_g15476_i8	Sh14Contig_78156	None
StHeBC4_u_c12903_g29964_i1	Sh14Contig_35346	None
None	Sh14Contig_62455	None
None	Sh14Contig_11292	None
StHeBC4_p_c12903_g43157_i2	Sh14Contig_5125	None
None	Sh14Contig_71030	None
StHeBC4_u_c12903_g18073_i1	Sh14Contig_20326	None
StHeBC4_p_c17480_g0_i1	Sh14Contig_62447	None
StHeBC4_p_c18975_g4_i6	Sh14Contig_44012	F7F22.15, related
StHeBC4_p_c12903_g32577_i4	Sh14Contig_50541	None
None	Sh14Contig_78156	None
StHeBC4_u_c12903_g32032_i1	Sh14Contig_20326	None
StHeBC4_u_c12903_g25724_i1	Sh14Contig_32318	None
StHeBC4_u_c13414_g0_i1	Sh14Contig_61194	None
None	Sh14Contig_43845	None
None	Sh14Contig_37580	None
StHeBC4_u_c12903_g1736_i12	Sh14Contig_28260	None
StHeBC4_p_c12903_g17146_i3	Sh14Contig_34580	None
StHeBC4_p_c12903_g33830_i2	Sh14Contig_22568	None
StHeBC4_p_c12903_g18700_i3	Sh14Contig_2850	None
None	Sh14Contig_61087	retrotransposon protein, putative, Ty3-gypsy subclass
StHeBC4_p_c12903_g208_i2	Sh14Contig_7920	None
StHeBC4_u_c14380_g6_i22	Sh14Contig_20089	None
StHeBC4_p_c12903_g22518_i1	Sh14Contig_39552	None
StHeBC4_u_c18188_g0_i1	Sh14Contig_30718	retrotransposon protein, putative, unclassified, expressed
StHeBC4_u_c12903_g35782_i1	Sh14Contig_27773	None
None	Sh14Contig_53940	None
None	Sh14Contig_29803	None

StHeBC4_p_c20119_g0_i1	None	None
StHeBC4_p_c12903_g26306_i42	None	None
StHeBC4_u_c12903_g15888_i8	None	None
StHeBC4_u_c12903_g34326_i2	None	None
StHeBC4_u_c22214_g0_i5	None	None
StHeBC4_u_c12903_g32907_i15	None	None
StHeBC4_p_c15477_g0_i2	None	None
StHeBC4_p_c12903_g18330_i2	None	None
StHeBC4_u_c20631_g2_i1	None	None
StHeBC4_u_c18975_g1_i1	None	None
StHeBC4_p_c12903_g33550_i2	None	None
StHeBC4_u_c20348_g0_i3	None	None
StHeBC4_u_c19161_g0_i1	None	None
StHeBC4_p_c18860_g2_i3	None	None
StHeBC4_p_c12903_g5434_i1	None	None
StHeBC4_p_c12903_g34427_i2	None	None
StHeBC4_u_c12903_g14239_i1	None	None
StHeBC4_p_c12903_g16488_i2	None	None
StHeBC4_u_c20110_g5_i1	None	None
StHeBC4_u_c17278_g0_i2	None	None
StHeBC4_p_c18569_g0_i2	None	None
StHeBC4_p_c12903_g15860_i11	None	None
StHeBC4_u_c12903_g16409_i1	None	None
StHeBC4_p_c12903_g5042_i2	None	None
StHeBC4_u_c12903_g42940_i10	None	None
StHeBC4_u_c18975_g1_i1	None	None
StHeBC4_u_c12903_g34427_i1	None	None
StHeBC4_u_c13012_g0_i1	None	None
StHeBC4_u_c20371_g0_i1	None	None
StHeBC4_u_c22472_g0_i4	None	None
StHeBC4_u_c12903_g34431_i3	None	None
StHeBC4_p_c18860_g2_i4	None	None
StHeBC4_p_c12903_g15230_i2	None	None
StHeBC4_u_c18860_g2_i48	None	None
StHeBC4_p_c12903_g8484_i1	None	None
StHeBC4_u_c18238_g1_i1	None	None
StHeBC4_u_c25350_g7_i2	None	None
StHeBC4_u_c12903_g29135_i2	None	None
StHeBC4_u_c13414_g0_i1	None	None
StHeBC4_p_c16184_g0_i1	None	None
StHeBC4_p_c12903_g27140_i4	None	None
StHeBC4_p_c12903_g18100_i3	None	None
StHeBC4_p_c26242_g21_i7	None	None
StHeBC4_u_c12903_g15860_i5	None	None
StHeBC4_p_c12903_g33449_i1	None	None
StHeBC4_u_c13012_g0_i1	None	None
StHeBC4_h_c10541_g0_i1	None	None
StHeBC4_u_c12903_g33428_i2	None	None
StHeBC4_u_c12903_g1552_i1	None	None

StHeBC4_p_c16622_g1_i2	None	None
StHeBC4_p_c12903_g8677_i10	None	None
StHeBC4_u_c10677_g0_i1	None	None
StHeBC4_p_c12903_g40108_i1	None	None
StHeBC4_u_c12903_g15860_i5	None	None
StHeBC4_p_c19033_g0_i1	None	None
StHeBC4_p_c12903_g33830_i1	None	None
StHeBC4_p_c12903_g11366_i6	None	None
StHeBC4_u_c12903_g25897_i6	None	None

860

Table S3. Chemocyanin variant calls for sequenced individuals. Individuals are coded as '1' if they possess the 'finger millet' allele or '0' if the allele is missing.

SampleID	Site	Host	Lat	Lon	Elevation_ft	Chemocyanin
SH009	Mumias	maize	0.3342	34.47782	4306	0
SH014	Mumias	maize	0.3342	34.47782	4306	0
SH023	Mumias2	maize	0.3038	34.50713	4299	1
SH027	Mumias2	maize	0.3038	34.50713	4299	0
SH031	Mumias2	maize	0.3038	34.50713	4299	0
SH035	Kibos	sorghum	-0.0363167	34.81567	3893	1
SH039	Kibos	sorghum	-0.0363167	34.81567	3893	0
SH042	Kibos	sorghum	-0.0363167	34.81567	3893	1
SH046	Kibos	maize	-0.0341417	34.81628	3917	0
SH055	Kibos	maize	-0.0341417	34.81628	3917	0
SH065	Muhoroni2	maize	-0.15125	35.19167	4239	0
SH070	Muhoroni2	maize	-0.15125	35.19167	4239	0
SH072	Muhoroni2	sugarcane	-0.15125	35.19167	4239	0
SH074	Muhoroni2	sugarcane	-0.15125	35.19167	4239	1
SH077	Muhoroni2	sugarcane	-0.15125	35.19167	4239	0
SH079	Chemelil	maize	-0.082375	35.13167	4176	0
SH087	Chemelil	maize	-0.082375	35.13167	4176	1
SH091	Chemelil2	sorghum	-0.0941667	35.12495	4060	0
SH097	Chemelil2	sorghum	-0.0941667	35.12495	4060	1
SH101	Chemelil2	sorghum	-0.0941667	35.12495	4060	0
SH103	Kisii	finger millet	-0.6138	34.73172	4925	1
SH104	Kisii	finger millet	-0.6138	34.73172	4925	1
SH105	Kisii	finger millet	-0.6138	34.73172	4925	1
SH106	Kisii	finger millet	-0.6138	34.73172	4925	1
SH107	Kisii	finger millet	-0.6138	34.73172	4925	1
SH108	Kisii	finger millet	-0.6138	34.73172	4925	1
SH109	Kisii	finger millet	-0.6138	34.73172	4925	1
SH110	Kisii	finger millet	-0.6138	34.73172	4925	1
SH111	Kisii	finger millet	-0.6138	34.73172	4925	1
SH112	Kisii	finger millet	-0.6138	34.73172	4925	0
SH113	Kisii	finger millet	-0.6138	34.73172	4925	0
SH114	Kisii	finger millet	-0.6138	34.73172	4925	0
SH115	Kisii	maize	-0.6133167	34.7318	4930	0
SH116	Kisii	maize	-0.6133167	34.7318	4930	0
SH117	Kisii	maize	-0.6133167	34.7318	4930	0
SH118	Kisii	maize	-0.6133167	34.7318	4930	0
SH119	Kisii	maize	-0.6133167	34.7318	4930	0
SH120	Kisii	maize	-0.6133167	34.7318	4930	0
SH121	Kisii	maize	-0.6133167	34.7318	4930	0
SH122	Kisii	maize	-0.6133167	34.7318	4930	0
SH123	Kisii	maize	-0.6133167	34.7318	4930	0
SH124	Kisii	maize	-0.6133167	34.7318	4930	0
SH125	Kisii	maize	-0.6133167	34.7318	4930	0
SH126	Kisii	maize	-0.6133167	34.7318	4930	0
SH127	Homa Bay	sorghum	-0.5839667	34.4762	4173	0

SH128	Homa Bay	sorghum	-0.5839667	34.4762	4173	0
SH129	Homa Bay	sorghum	-0.5839667	34.4762	4173	0
SH130	Homa Bay	sorghum	-0.5839667	34.4762	4173	0
SH131	Homa Bay	sorghum	-0.5839667	34.4762	4173	0
SH132	Homa Bay	sorghum	-0.5839667	34.4762	4173	0
SH133	Homa Bay	sorghum	-0.5839667	34.4762	4173	1
SH134	Homa Bay	sorghum	-0.5839667	34.4762	4173	0
SH135	Homa Bay	sorghum	-0.5839667	34.4762	4173	0
SH136	Homa Bay	sorghum	-0.5839667	34.4762	4173	0
SH137	Homa Bay	sorghum	-0.5839667	34.4762	4173	0
SH138	Homa Bay	sorghum	-0.5839667	34.4762	4173	0
SH139	Homa Bay 2	maize	-0.5834	34.47635	4161	0
SH140	Homa Bay 2	maize	-0.5834	34.47635	4161	0
SH141	Homa Bay 2	maize	-0.5834	34.47635	4161	0
SH142	Homa Bay 2	maize	-0.5834	34.47635	4161	1
SH143	Homa Bay 2	maize	-0.5834	34.47635	4161	1
SH144	Homa Bay 2	maize	-0.5834	34.47635	4161	0
SH145	Homa Bay 2	maize	-0.5834	34.47635	4161	1
SH146	Homa Bay 2	maize	-0.5834	34.47635	4161	0
SH147	Homa Bay 2	maize	-0.5834	34.47635	4161	0
SH148	Homa Bay 2	maize	-0.5834	34.47635	4161	0
SH149	Homa Bay 2	maize	-0.5834	34.47635	4161	0
SH150	Homa Bay 2	maize	-0.5834	34.47635	4161	0

863
864

865 **FIGURE LEGENDS**

866

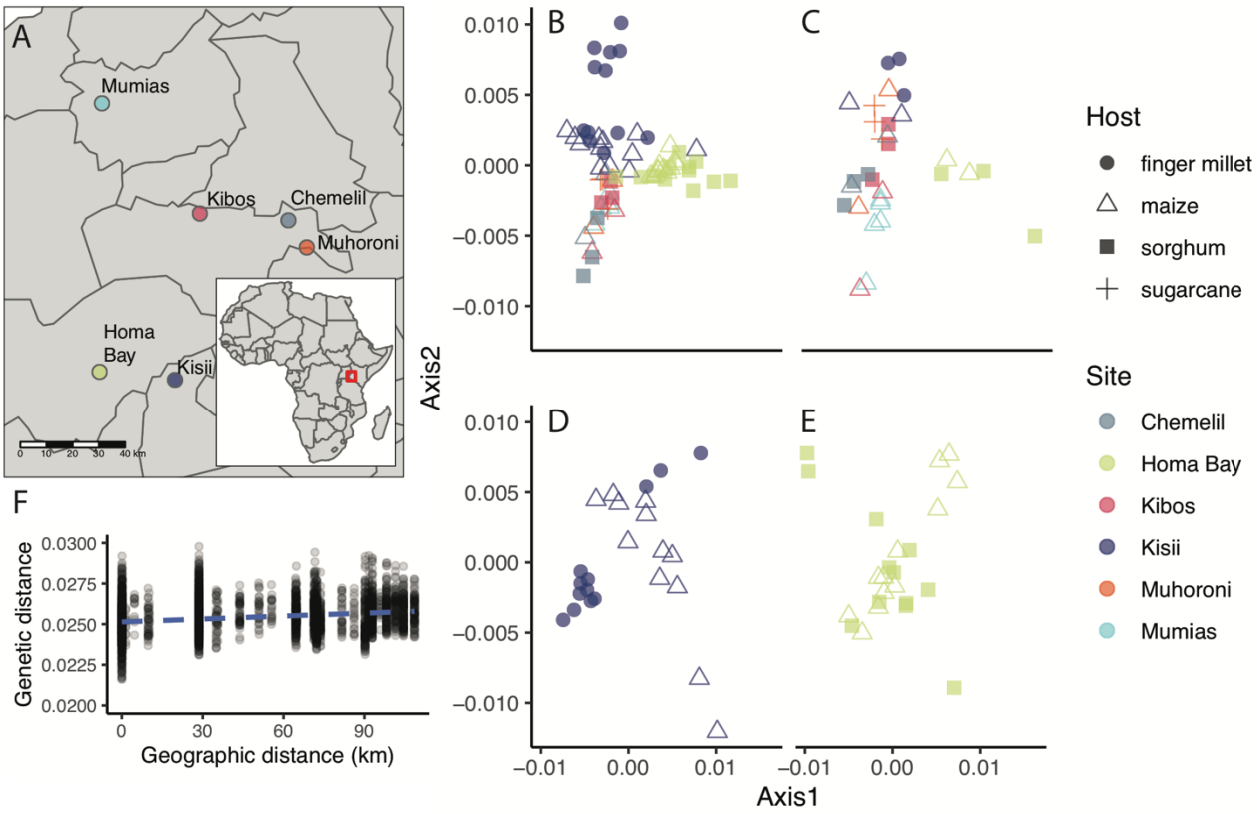

867

868 **Figure 1.** Population genomics of *S. hermonthica* from western Kenya. A) Map of the six

869 sampling locations. (B-E) Principal Coordinates Analysis (PCoA) based on *k*-mer-derived

870 genomic distances, performed separately for B) all sampled individuals (*n* = 68), C) five

871 individuals per location (*n* = 30), D) individuals from Kisii (*n* = 24), and E) individuals from Homa

872 Bay (*n* = 24). F) Genetic vs. geographic distance. Genetic distance was based on 31-mers. The

873 dashed blue line indicates expectations from the best fit line (y = 0.000013 * km + 0.0246; R^2 =

874 0.05) for *n* = 4,556 pairwise comparisons among different individuals.

875

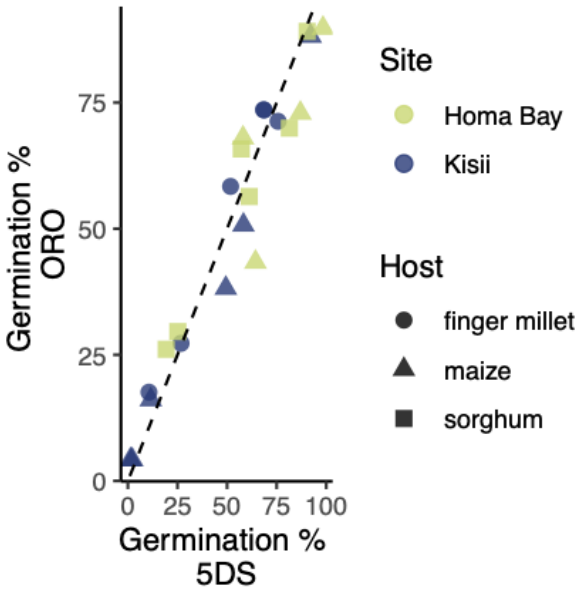

Figure 2. Germination response variation in Homa Bay and Kisii populations. Seeds from *n* = 6 individuals per unique site and host were tested in response to synthetic strigolactones orobanchol (ORO, 0.01 uM) and 5-deoxystrigol (5DS, 0.01 uM). The dashed line indicates the expectation if the percent germination in response to the two different germination stimulants is identical.

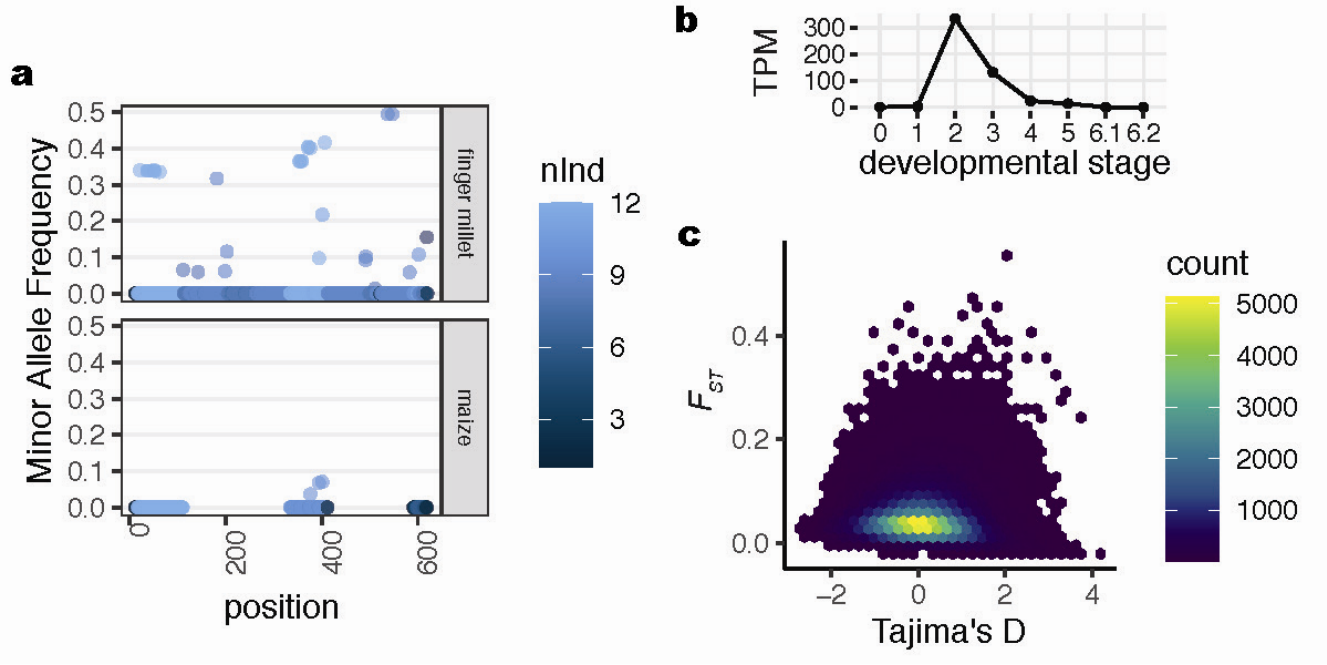

Figure 3. Genetic variation in *Striga hermonthica* from Kisii, Kenya. (a) Presence/absence variation across the chemocyanin precursor transcript (StHeBC4_h_c11261_g0_i1), for *n* = 12 individuals per host (finger millet or maize). If the locus is not present in any of the sequenced individuals, no data point is shown, otherwise each point is colored according to the number of individuals (nInd) with data for the position. (b) Gene expression data in transcripts per million (TPM) from the PPGPII dataset for the chemocyanin precursor transcript across six stages of haustorial development (0: imbibed seed; 1: germinated seedling after exposure to GR24; 2: germinated seedling after exposure to DMBQ; 3: ~48 hrs post-attachment; 4: ~72 hrs post-attachment; 5: late post-attachment; 6.1: vegetative structures; 6.2: reproductive structures). (c) Distribution of Tajima's D and F_{ST} values across 154,722 non-overlapping 1-kb windows. Only windows with data for more than 50% of sites are shown, excluding impacts of structural genetic variation as in (a). Tajima's D for the chemocyanin was -1.7.